RESEARCH REPORT

Contract no. 93/5.10.2011

EXPLORATORY RESEARCH PROJECTS (IDEI)

Project:

The geomagnetic field under the heliospheric forcing. Determination of the internal structure of the Earth and evaluation of the geophysical hazard produced by solar eruptive phenomena

Stage V (2015)

Project Director,

Dr. Crişan Demetrescu
Corresponding Member of the Romanian Academy

December, 2015

Cuprins

Introduction

The proposed research aims at achieving an understanding of the space weather effects on conducting structures inside the Earth and on the surface electric field, with applications to a better knowledge of the internal structure of the Earth at continental (Europe) and country scales, on one hand, and to estimating the geophysical hazard of space weather at midlatitudes, on the other. The main objectives are:

1. To derive the magnetic and electrical properties of the terrestrial lithosphere and mantle at continental and Romanian territory scales;

2. To analyze solar eruptive processes and solar wind components responsible for geomagnetic hazardeous activity (geomagnetic storms and substorms) in the time interval 1964-2014;

3. To model the geoelectrical field at the Earth's surface as produced by various magnetospheric and ionospheric current systems;

4 To evaluate the geophysical hazard for technological networks associated to variations of the geoelectric field during geomagnetic disturbances linked to the interaction of solar coronal mass ejections and high speed streams with the magnetosphere.

The initial contract underwent alterations because of budget cuts, so for 2015, according to the additional agreement signed with UEFISCDI, the objectives read:

- Determination of magnetic and electric structure of terrestrial lithosphere and mantle at Romanian territory and European continental scales;
- Analysis of solar eruptive processesand solar wind, responsible for the hazardeous geomagnetic activity (geomagnetic storms with $-150 < Dst < -50$ nT), in the solar cycle 23;
- Modeling of geophysically induced currents (GIC) by geomagnetic storms produced by solar eruptive phenomena, stage 2015;
- Preparing the research report and dissemination of results.

The research report for the stage 2015 is structured in chapters, according to the work plan, as follows:

In *Chapter I*, entitled "**New geomagnetic and magneto-telluric measurements in Romania**" the geomagnetic measurements carried out in 2014 at the 26 repeat stations of the National secular variation network and at the Surlari geomagnetic observatory, as well as the results of two magneto-telluric determinations carried out in the Vrancea active seismic zone, are described.

In *Chapter II*, entitled "**Magnetic and electric structure of terrestrial litosphere and mantle at Romanian territory and continental scales. Improving the resistivity model based on the new determined values**", two models of the distribution of electric properties of lithosphere and mantle are presented, one for the European continent, using data from the geomagnetic observatory network and data for a number of geomagnetic storms, and a second one, for the Romanian territory, using magneto-telluric measurements. In the first case the magnetic/electromagnetic induction model, previously devised by research team members, was used. In the second case the electric structure of the crust on the Romanian territory is presented, as a block model with vertical variation of the electrical resistivity in each block.

In *Chapter III*, entitled "**Analysis of solar eruptive processes and of solar wind, responsible for the moderate geomagnetic activity (geomagnetic storms with minimum Dst between -50 nT and -150 nT) during solar cycle 23**", Solar eruptive processes and High speed streams in the solar wind that generated moderate geomagnetic storms in the solar cycle 23 are presented. The effects of the mentioned processes on the magnitude of the storm characterized by the geomagnetic index Dst have been studied by means of a correlation analysis of this index with several quantities that characterize the two types of processes (speed of the coronal mass ejection, the kinetic energy of the coronal mass ejection, the product of the speed and the associated magnetic field, the speed of the solar wind high speed stream, the product of the speed and the associated magnetic field, the speed jump that characterize the high speed stream).

In *Chapter IV***,** entitled "**Modelling of geophysically induced currents (GIC) by geomagnetic storms produced by solar eruptive phenomena, stage 2015**", results for the European continent are presented, in case of nine intense storms of the solar cycle 23 (Dst<-150 nT), based on recordings provided by the 29 European geomagnetic observatories of the INTERMAGNET project. For the case of the most intense storm in the solar cycle 23, the November 20-21, 2003 one, with Dst = -422 nT, a study of the sources of the geomagnetic variations recorded by observatories (ionospheric and magnetospheric currents), as well as a study on the evolution of the induced electrical field by the storm time geomagnetic

variations were undertaken. A result concerning the geographical distribution of the maximum electric field induced by each of the magnetic storms of the study is presented as well.

In *Chapter V*, entitled ”**Dissemination of results**”, the list of published papers and of papers presented at scientific meetings during the year 2015 is given. The web page of the project has been updated. The address is: http://www.geodin.ro/IDEI2011/engl/index.html.

Chapter I. New geomagnetic and magneto-telluric measurements in Romania

1.1. Geomagnetic measurements

The geomagnetic measurements were taken at the 26 repeat stations that compose the so-called The National Secular Variation Network, as well as at the Surlari Geomagnetic Observatory. The field measurement campaign took place in the time intervals 05.08-19.08.2015 and 25.08-03.09.2015. In Fig. 1.1.1 the way the territory has been covered during this campaign is illustrated.

Determinations of the horizontal component H, total field intensity F, magnetic declination D, and magnetic inclination I have been carried out. In parallel with the absolute measurements, recordings of the field evolution, through the four elements X, Y, Z, and F, have been carried out. A DI-Flux LEMI 024 theodolite, two QHM magnetometers, a Geometrics G-856 and a recording LEMI-18 fluxgate magnetometer have been deployed.

The determined values were corrected for the diurnal variation and reduced to the time of the first reading of the series of determinations stipulated in the measurement protocol, by means of continuous recordings provided by the Surlari geomagnetic observatory. Then the values were processed to obtain values for the middle of the year 2014 (the geomagnetic epoch 2014.5), having in view the delay of about one year that affects observatory annual mean values against which the field data are reduced. In Fig. 1.1.2 the maps of the geographical distribution of the geomagnetic elements H, Z, D, and F are presented, reduced to the epoch 2014.5 for which the necessary data from the Surlari geomagnetic observatory were the definitive ones.

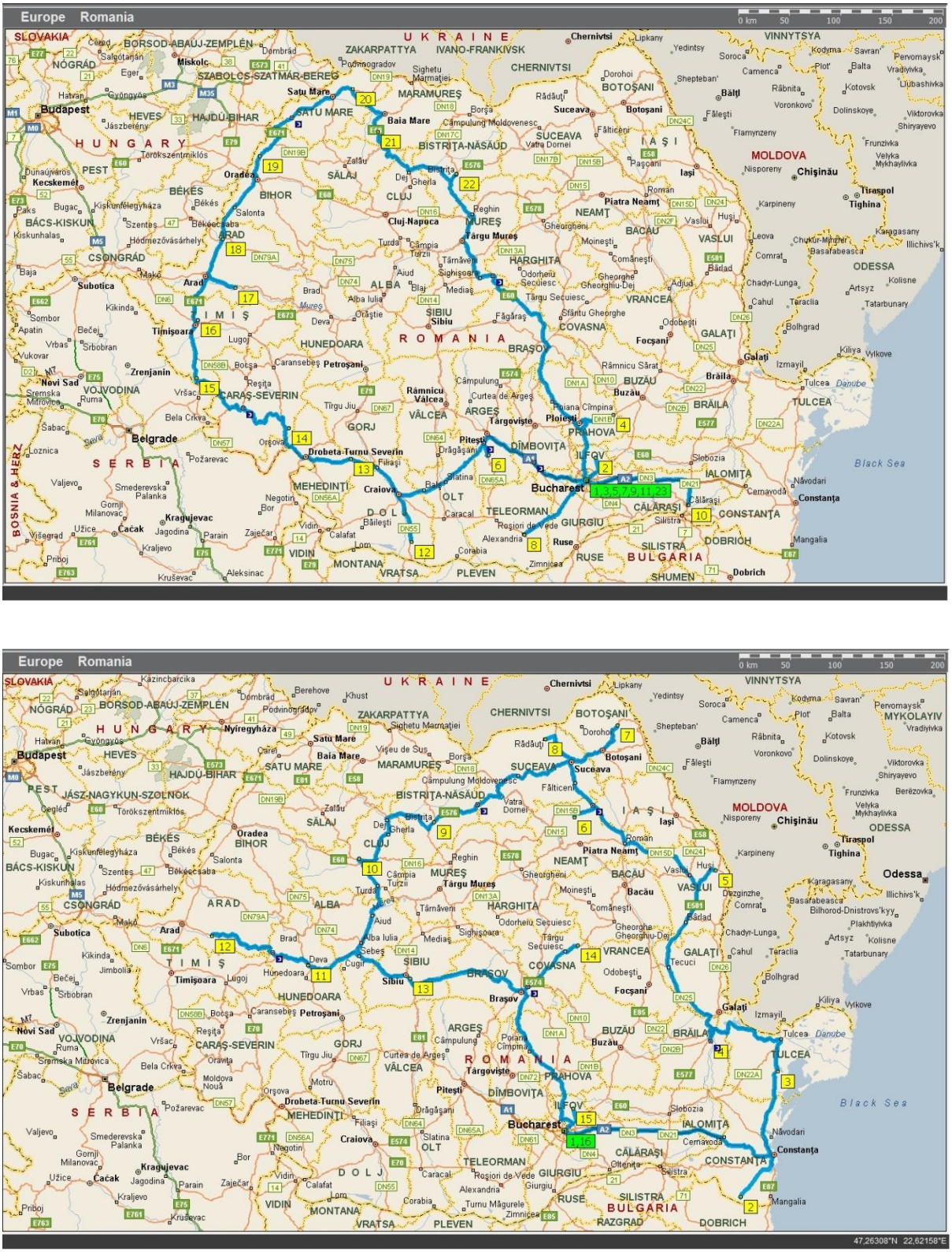

Fig. 1.1.1. The way the station network was covered in the time intervals 05.08-19.08.2015 (above) and 25.08-03.09.2015 (below)

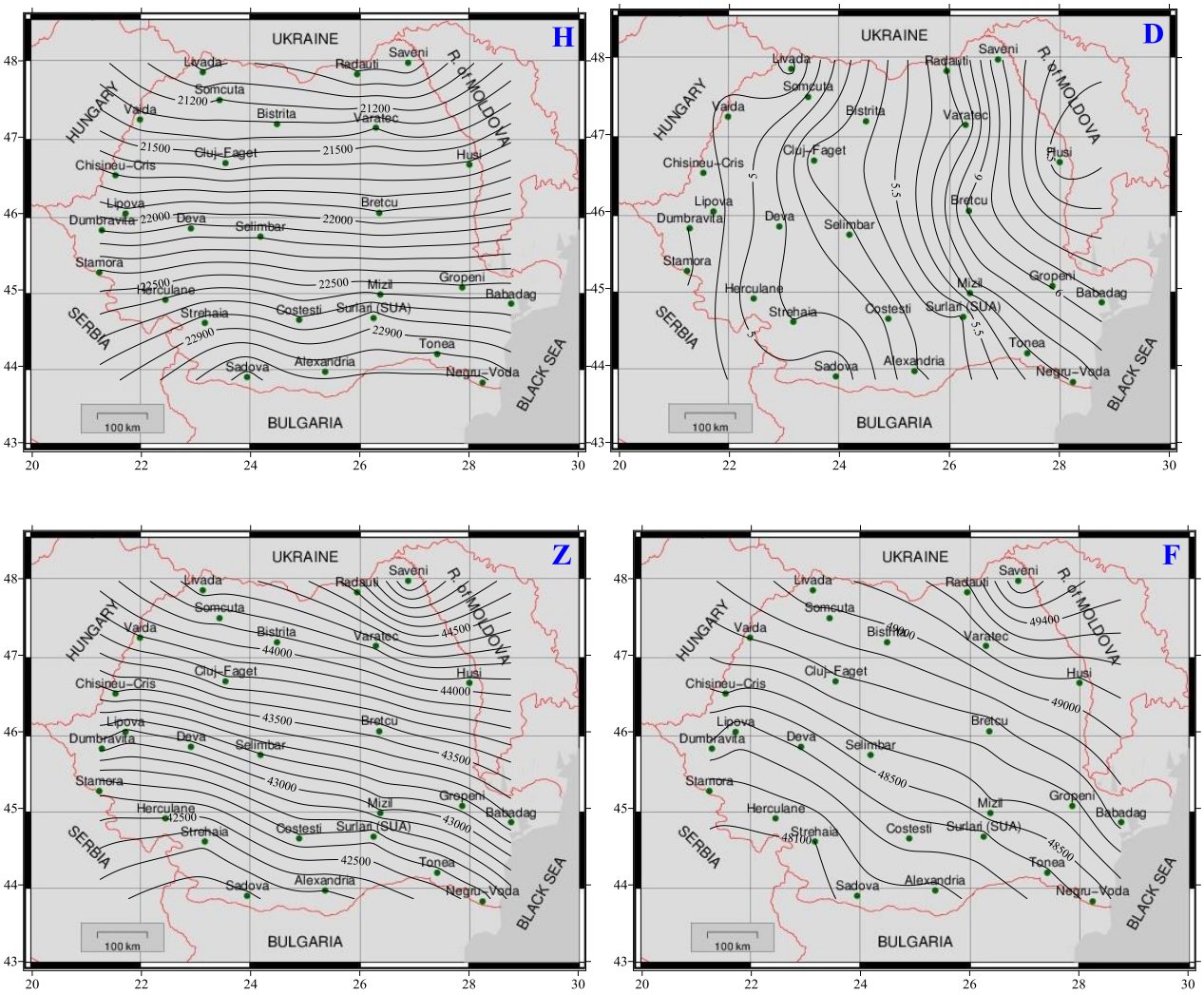

Fig. 1.1.2. The geographical distribution on the Romanian territory of the geomagnetic elements H, D, Z, and F at epoch 2014.5 (measurements carried out in 2015). The repeat stations of the National secular variation network are marked by symbols

1.2. Magneto-telluric measurements

1.2.1. Magneto-telluric measurements în the Vrancea active seismogenic area, Buzau county

To get information on the vertical distribution of the electrical resistivity, during September – October 2015 two magneto-telluric soundings (MTS1 and MTS2) were carried out in the Vrancea active seismogenic area, in the vicinity of Lopătari and Vintilă Vodă localities (Fig. 1.2.1).

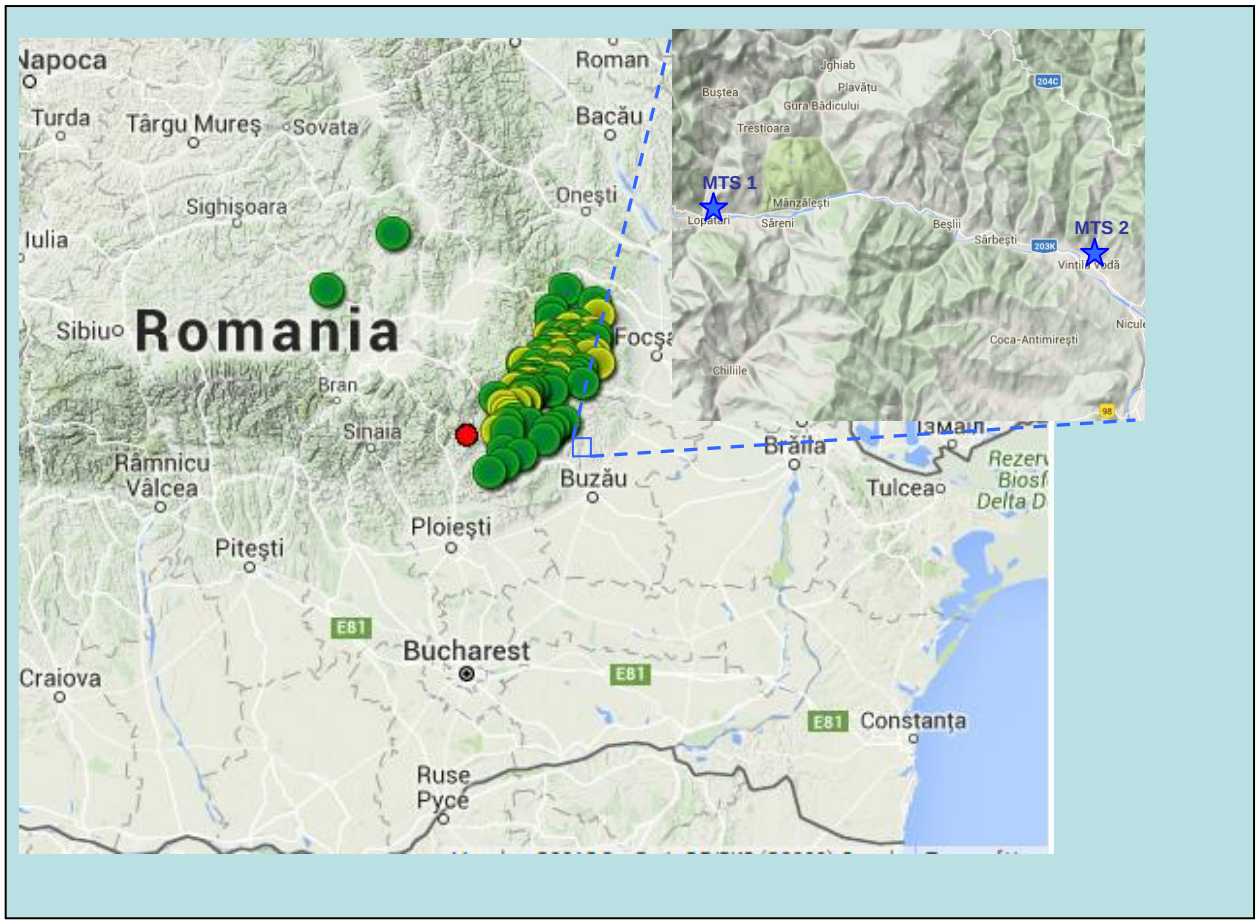

Fig. 1.2.1. Location map for the two mageto-telluric (MT) stations (MTS1-Lopatari and MTS 2-Vintilă Vodă) in the active Vrancea seismic area; green, yellow and red circles stand for epicentres of earthquakes occurred in 2015 (modified after INFP)

1.2.1.1. Methodology of acquisition, processing, modelling and 1-D inversion of resistivity curves

A multi-channel magnetotelluric system (GMS-06) produced by METRONIX company, Germany, was used. The central unit ADU-06 has 5 channels at which 4 un-polarized sensors for electric field recording and 3 magnetic sensors (induction coil) for magnetic field recording are connected. To get information at a crustal level, the recording of magneto-telluric series (Ex, Ey, Bx, By şi Bz) took approximately 20 days, and the frequency range recorded was of 10Hz - 5.10^{-4} Hz.

The observation data are stored either in the internal "flashdisk" memory, or directly on the control computer (Laptop) HDD, on which the MAPROS code is installed. This code runs under Windows 95 and controls the following operations:

1. Semi-automatic settings of Ex, Ey, Hx, Hy, Hz sensors;

2. Real-time data acquisition and processing;
3. Robust estimation of the magnetotelluric transfer functions Zxy, Zyx and of the geomagnetic transfer functions Txy ,Tyx;
4. Real-time time series representation for resistivity and phase curves for MTS1- Lopătari (Fig. 2.2.2) and MTS2- Vintilă Vodă (Fig. 2.2.3).

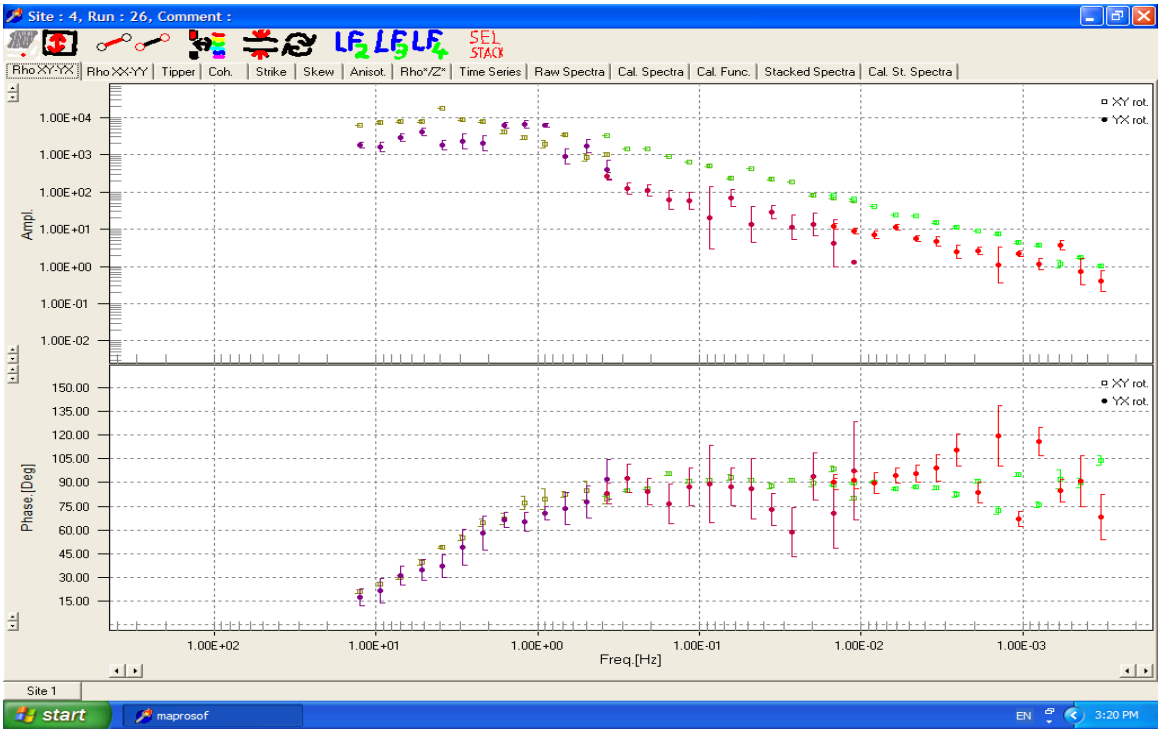

Fig.1.2.2. Resistivity (upper plot) and phase (lower plot) distributions versus frequency for MTS1-Lopătari

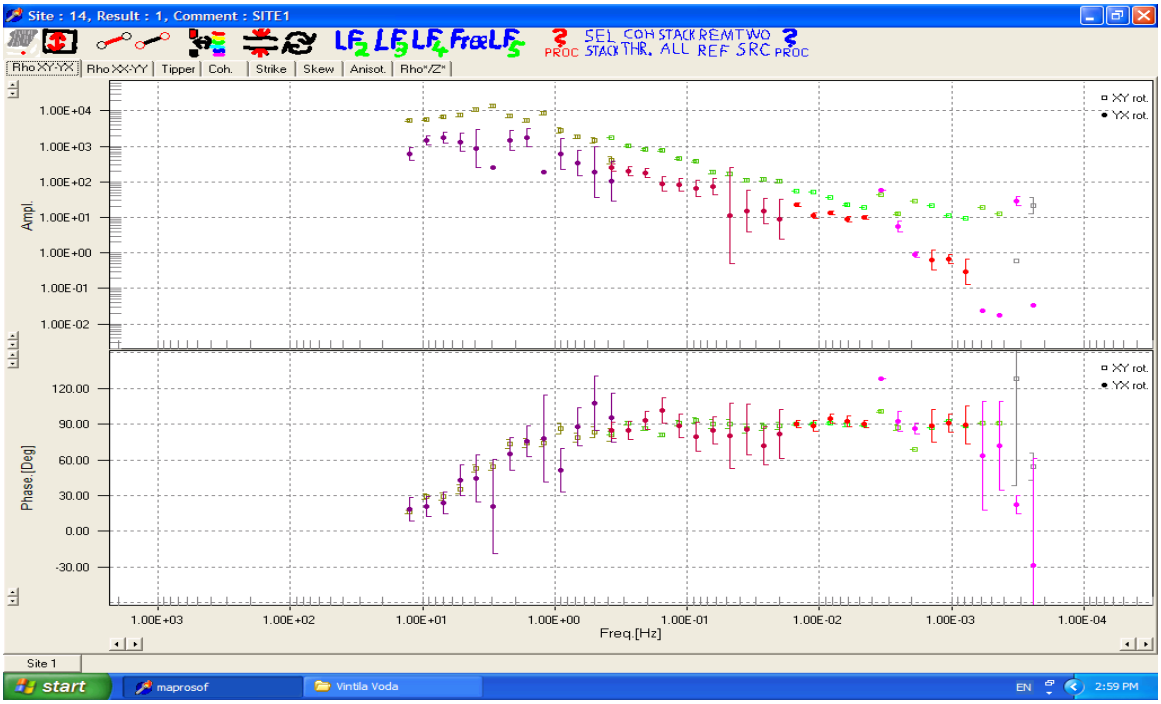

Fig. 1.2.3. Resistivity (upper plot) and phase (lower plot) distributions versus frequency for MTS2- Vintilă Vodă

1.2.2. Results

The vertical distribution of resistivities at the two measurement locations were obtained by means of a 1-D inversion code. The results are presented as a single model (Fig. 1.2.4) for both magneto-telluric soundings, as the resistivity curves in the two case are similar, reflecting a near identical geological structure, characteristic to the foreland of the Eastern Carpathins bending zone.

The model has been obtained after several iterations, by means of the IPI inversion code, and represents most probably the real image of the geological structure in the investigated area (The foreland of the Eastern Carpathians bend), as there is only 2% difference between experimental and calculated response functions. According to the Fig. 1.2.4 caption, the model shows the following thicknesses: approximately 9 km for the nappe system of the Carpathian flisch; 4.6 km for the sedimentary cover of the Moesian Platform; 27 km for the crystalline basement. The corresponding resistivities are: 3100 Ωm, 120 Ωm, 400 Ωm. A low resistivity of 0.4 Ωm is associated to the transition crust – upper mantle. In the study area the crust is approximately 40 km thick, in agreement with data for the Vrancea area (Stanica et al., 2004).

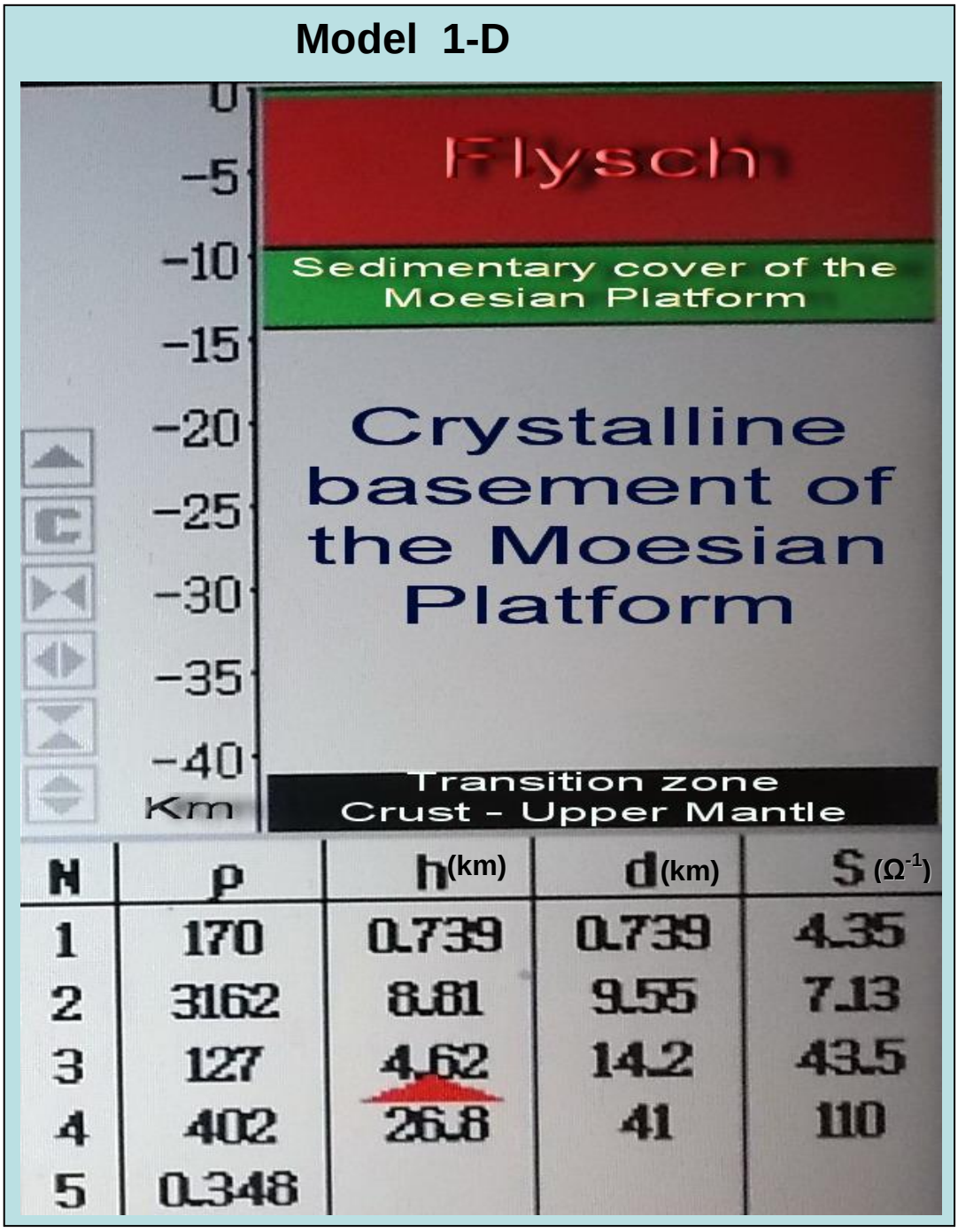

N	ρ	h(km)	d(km)	S (Ω^{-1})
1	170	0.739	0.739	4.35
2	3162	8.81	9.55	7.13
3	127	4.62	14.2	43.5
4	402	26.8	41	110
5	0.348			

Fig. 1.2.4. 1-D model for MTS1and MTS2; N-number of layers, ρ- apparent resistivity, h-layer thickness, d- depth, S-conductance

Chapter II. Magnetic and electric structure of terrestrial litosphere and mantle at Romanian territory and continental scales. Improving the resistivity model based on the new determined values

2.1. Model at the European continental scale, based on analysis of intense geomagnetic storms in solar cycle no. 23

In the previous stages of the contract we used the so-called „magnetic and electromagnetic induction mehod", previously worked out by the contract team members, to the case of a major geomagnetic storms of the solar cycle 23, more precisely for 9 of them, illustrated in Fig. 2.2.1 by means of the geomagnetic index Dst. In the stage report for the year 2014 the study was done for the six days encompasing the storm. The results we obtained determined us to continue the study using only the main phase of the storm, developing in only 6 to 13 hours. We remind that 1-minute recordings from the 29 European observatories included in the INTERMAGNET network were used for the study. The principle of the method is shortly explained in the following.

2.1.1. The principle of the magnetic induction method

The method used in the present work (see the Phase 2013 report) is based on the observation that an external variable field induces inside the Earth variable magnetic fields not only through electromagnetic induction in conductive structures of the crust and mantle, but also by magnetic induction in rocks above the Curie temperature. In the pure magnetic induction case, the temporal variation of the field components at a certain observation point is given by a linear combination of the components of the inducing magnetic force. The calculated values of the model represent the component of the observed signal produced by pure magnetic induction, while the residuals contain the information related to the electromagnetic induction in the Earth at the given point. The model coefficients can be determined by a least squares procedure and mapped, resulting in images of the lateral (geographical) distribution of magnetic properties that characterise the rock volume above the Curie temperature (generaly the crust).

In case of **electric properties** of crust and mantle, the residual of the induction model for the **vertical component of the field** is used. The latter responds to the electromagnetic induction in the electrically conducting crustal and mantle structures to a greater extent than the horizontal component. As the induction electromotive force is given by the negative time

derivative of the inducing magnetic field, the latter should correlate with the observed residual. The working relationship is:

$$-\dot{Z}_{sursa}(t) = L \cdot \dot{Z}rez(t) + R \cdot Zrez(t),$$

where $-\dot{Z}_{sursa}$ is the negative time derivative of the vertical component produced by the inducing source, and Zrez is the residual of the induction model applied to the Z component recorded at the observation point. L and R, the electrical inductance and, respectively, the resistance that characterise the crust and mantle under the given observatory, can be determined for each observatory by means of the least squares method, for the given time interval. Mapping of the obtained values reflects the lateral distribution of the Earth interior electric properties. The mapped values are relative, the maps reflecting, as was also the case of magnetic properties of the crust (the 2012 Report), lateral variations of the parameters L and R, not real (absolute) values. Also, the obtained information regards a large depth range, from the surface to mantle depths, as a function of the penetration depth of the external disturbance.

2.1.2. Results

In Fig. 2.1.1 the nine storms included in the study are presented, and in Fig. 2.1.2 the obtained results, as maps of normed values of the resistance R calculated using Dst and recorded disturbing field values. Significant differences between maps can be noticed, that for now we put on the different depth penetration of the electromagnetic signal produced by the corresponding storms. We have in mind the different time interval length of the storm main phase (marked on the figure), on one hand, and different morphologies of the main phase, on the other.

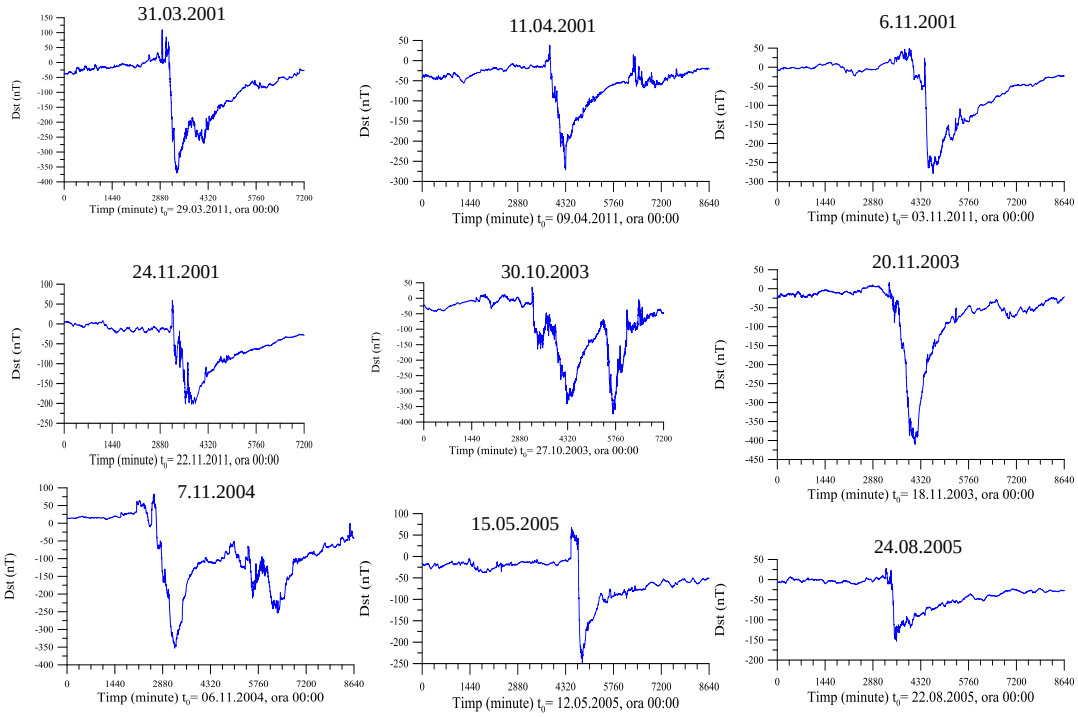

Fig. 2.1.1. The variation of the Dst geomagnetic index for the analysed geomagnetic storms

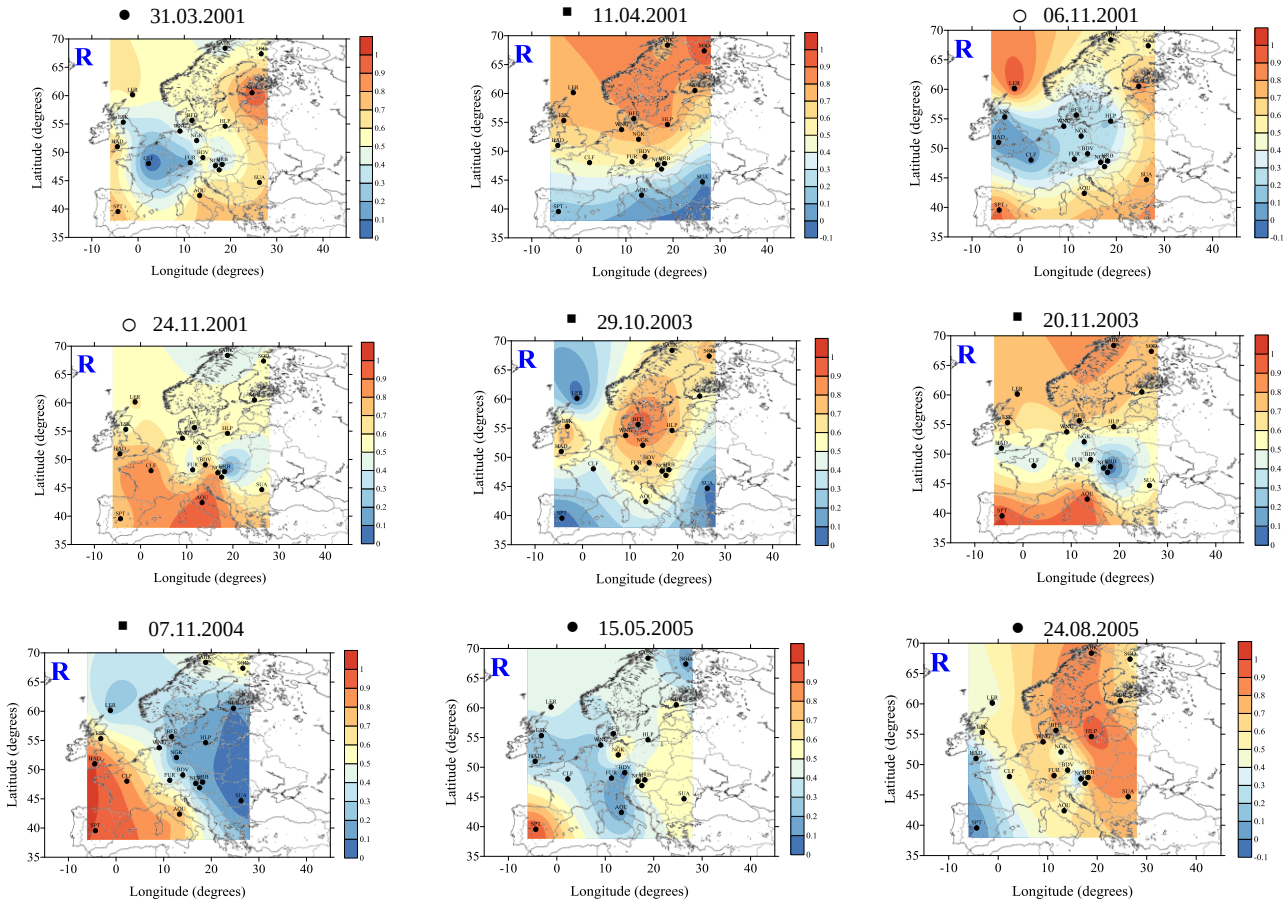

Fig. 2.1.2. The geographical distribution of the R parameter, calculated for the main phase of the storm. Duration: • 6 hours; ■ 10 hours; ○ 13 hours

2.2. 1-D models of the resistivity distribution on the Romanikan territory

In this stage of the project we show a synthetic model for the vertical distribution of resistivity of crust and upper mantle rocks on the Romanian territory, based on magneto-telluric soundings from the data archives of the Institute of Geodynamics (Stanică and Stanică, 1993; Stanică et al., 1999), and on studies reported in the previous and the present stages of the contract. The model describes the vertical variation of resistivity as 1-D sub-models for a number of parallelipipedic volumes in which the Romanian territory has been divided, represented by the grid of Fig. 2.2.1. The grid, superposed on the map of magneto-telluric geotraverses that have been used in modelling, allows to detail and to multiply information that actually refers to the main tectonic units on the Romanian territory, of larger dimensions. The digits that mark the grid squares allow retrieving the corresponding vertical 1-D model. The six types of vertical distribution of resistivity are shown in Figs. 2.2.2 – 2.2.7. They refer, respectively, to the East European Platform + Scythian Platform + Eastern Carpathians Foredeep + North Dobrudjan Orogen, model 1, Transylvanian Depression, model 2, Pannonian Depression, model 3, Moesian Platform + Southern Carpathians Foredeep, model 4, Eastern Carpathians + Neogene Volcanic Chain, model 5, and Southern Carpathians, model 6.

Based on data described above, a map of the geographical distribution of crust and upper mantle resistivity was constructed, wit a resolution that corresponds to the grid of Fig. 2.2.1, map that will be used, together with the information provided by the Surlari Geomagnetic Observatory and repeat stations of the National Secular Variation Network, for the study of the induced hazard by the so-called space weather (for instance geomagnetic storms). The map is shown in Fig. 2.2.8.

References

Stănică D., Stănică Maria, An electrical resistivity lithospheric model in the Carpathian Orogen from Romania. Physics of the Earth and Planetary Interiors, 81(1993), 99-105. Crustal - Scale Studies, Elsevier Science Publishers B. V., Amsterdam, 1993, ISSN: 0031-9201.

Stănică M., Stănică D., Marin-Furnică C., The Placement of the Trans-European Suture Zone by Electromagnetic Arguments on the Romanian Territory. Earth, Planets and Space, 51, 1073-1078, 1999.

Dumitru Stănică, Maria Stănică, Luigi Piccardi, Emanuele Tondi, Giuseppe Cello: Evidence of geodynamic torsion in the Vrancea zone (Eastern Carpathians), Rev. Roum. de GEOPHYSIQUE, Vol. 48, 2004.

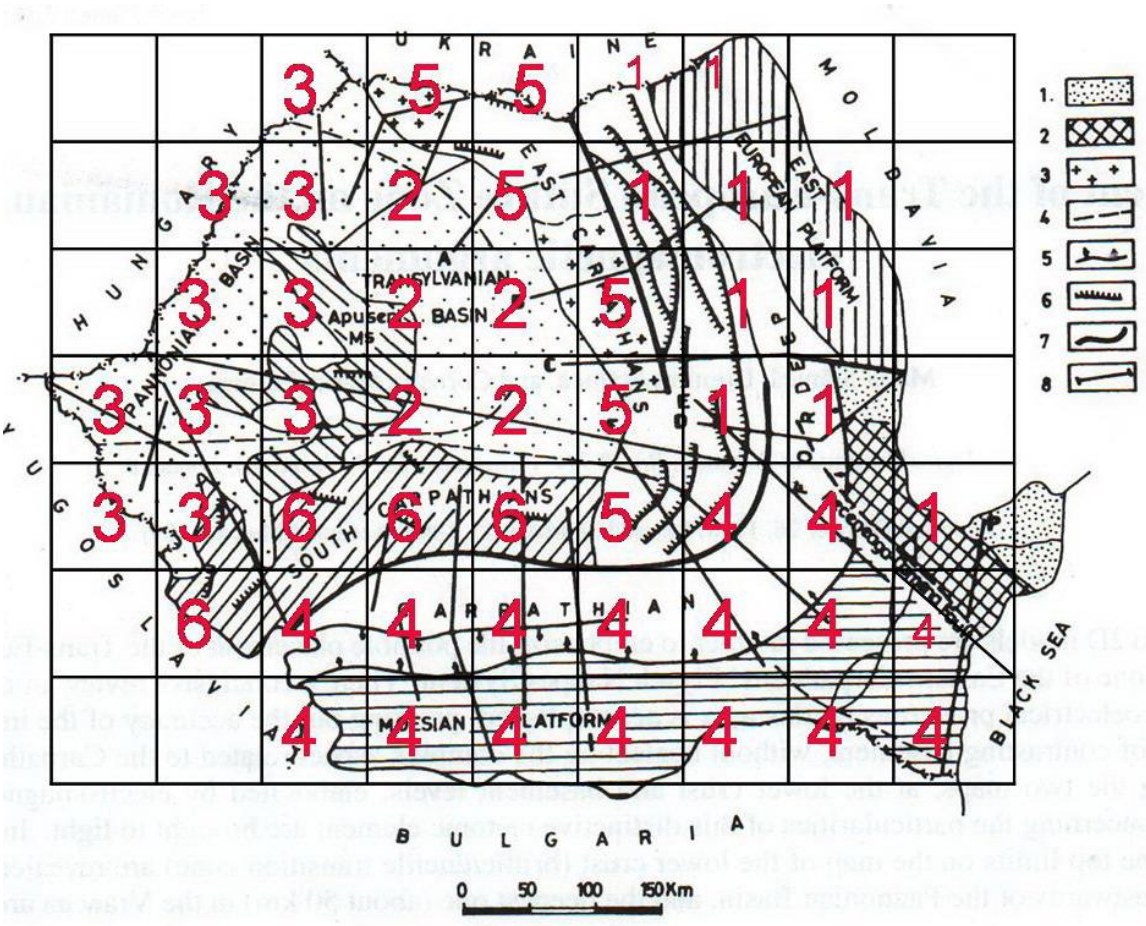

Fig. 2.2.1. Map showing location of magneto-telluric geotraverses in Romania (after Stanica et al., 1999). 1-Scythian Platform; 2- North Dobrudjan Orogen; 3- neogene volcanic chain; 4-deep fault; 5-flexure; 6-overthrust; 7- Carpathian electrical conductivity anomaly; 8- MT profile. Grid with red digits corresponds to the six 1-D models for the vertical variation of electric properties

East European Platform

1-D resistivity model (ρ) in lithosphere

Layers	ρ[Ωm]	H [km]	Observations
1	10	10	Sedimentary cover of the platform
2	1000	35	Crystalline basement
3	10	10	Crust-upper mantle transition zone
4	500	120	Upper mantle
5	10		Asthenosphere

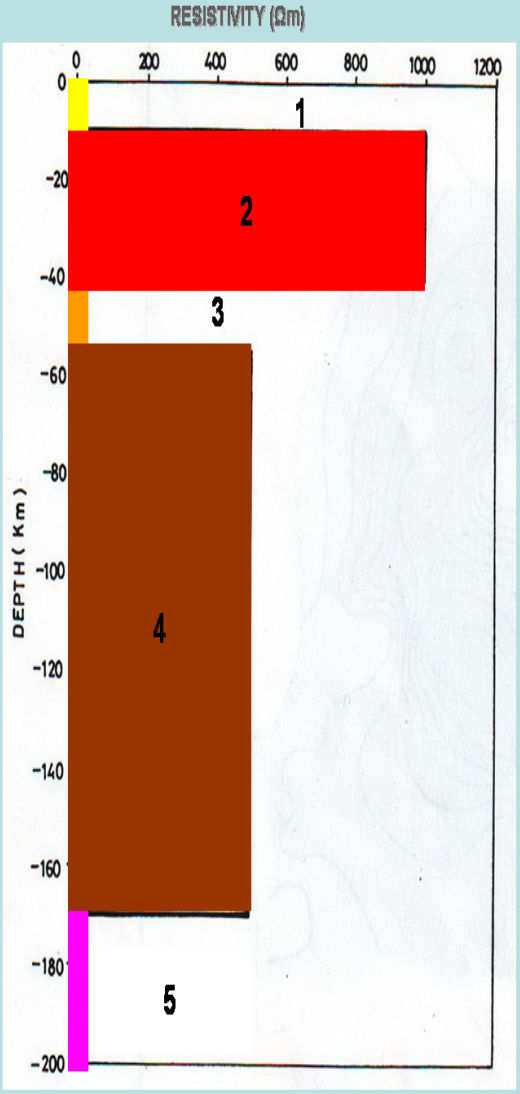

Fig. 2.2.2. MODEL 1: 1-D lithospheric resistivity model for the East European Platform + Scythian Platform + Eastern Carpathians Foredeep + North Dobrudjan Orogen

Transylvanian Depression

1-D lithospheric resistivity (ρ) model

Layers	ρ [Ωm]	H [km]	Observations
1	5	5	Post-tectogenetic sedimentary cover
2	500	2	Central-East Carpathian Nappes Systems
3	700	24	Crystalline basement
4	10	10	Crust-upper mantle transition zone
5	500	40	Upper mantle
6	10		Asthenosphere

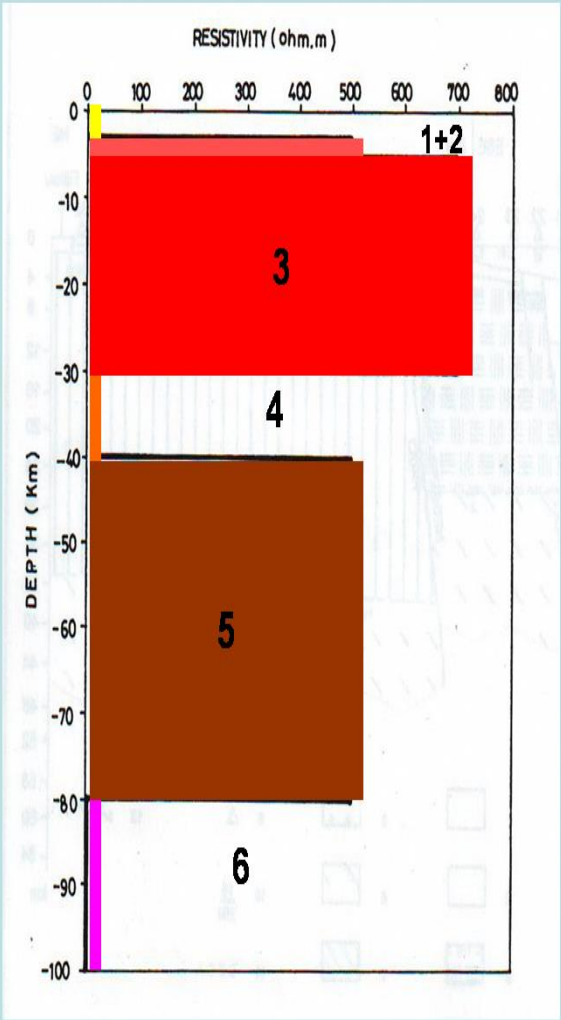

Fig. 2.2.3. MODEL 2: 1-D lithospheric resistivity model for the Transylvanian Depression

Pannonian Depression

1-D resistivity model (ρ) in lithosphere

Layers	ρ [Ωm]	H [km]	Observations
1	5	4	Sedimentary cover
2	700	16	Crystalline basement
3	10	10	Crust-upper mantle transition zone
4	500	30	Upper mantle
5	10		Asthenosphere

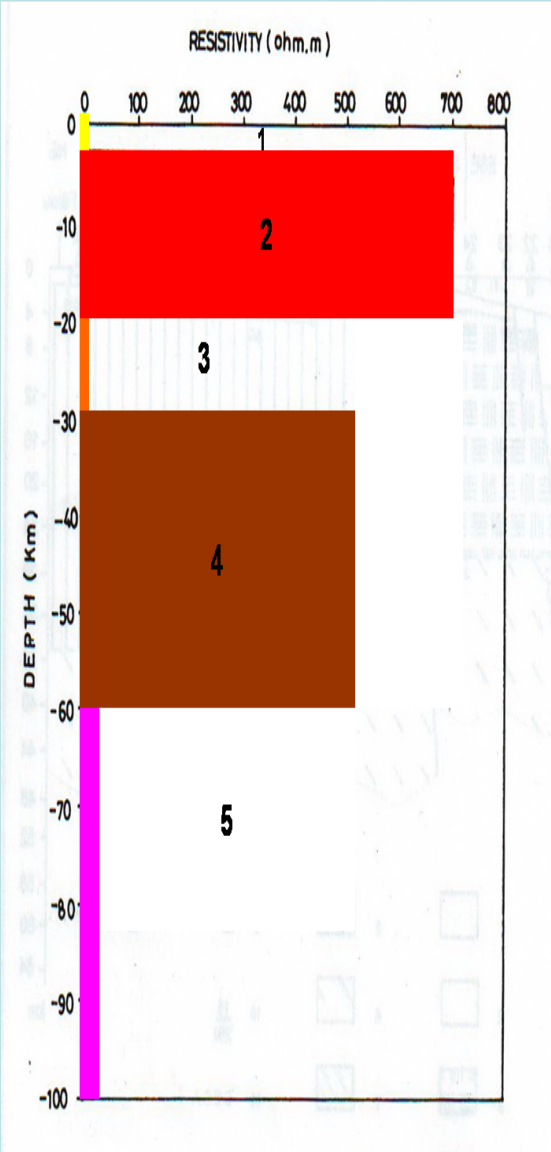

Fig. 2.2.4. MODEL 3: 1-D lithospheric resistivity model for the Pannonian Depression

Moesian Platform

1-D resistivity model (ρ) in lithosphere

Layers	ρ [Ωm]	H [km]	Observations
1	10	10	Sedimentary cover of the platform
2	1000	30	Crystalline basement
3	10	10	Crust-upper mantle transition zone
4	500	80	Upper mantle
5	10		Asthenosphere

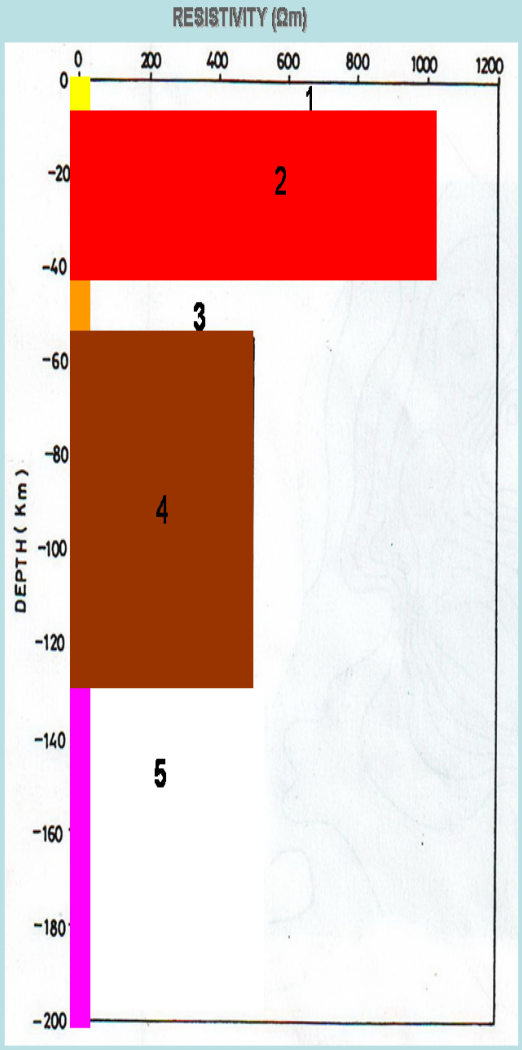

Fig. 2.2.5. MODEL 4: 1-D lithospheric resistivity model for the Moesian Platform + Southern Carpathians Foredeep

East Carpathians

1-D resistivity model (ρ) in lithosphere

Layers	ρ[Ωm]	H [km]	Observations
1	100	3	Central East Carpathian Nappes System
2	80	5	Flysch Nappes System
3	10	4	Sedimentary Cover
4	1000	30	Crystalline basement of the East- European Platform
5	10	10	Crust-upper mantle transition zone
6	500	120	Upper mantle
7	10		Asthenosphere

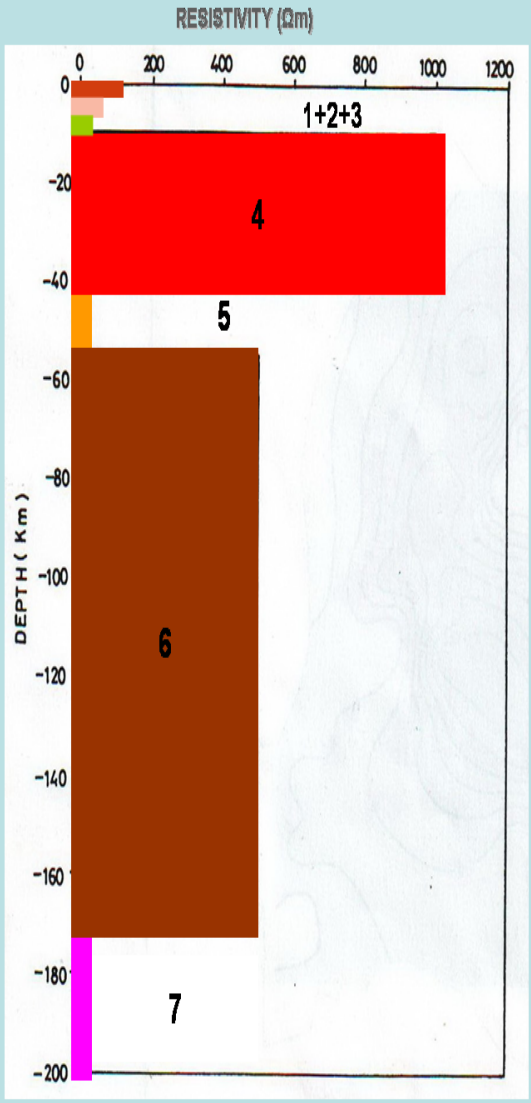

Fig. 2.2.6. MODEL 5: 1-D lithospheric resistivity model for the Eastern Carpathians + Neogene Volcanic Chain

South Carpathians

1-D resistivity model (ρ) in lithosphere

Layers	ρ [Ωm]	H [km]	Observations
1	100	6	Getic Nappes
2	300	7	Danubian Unit
3	1000	30	Crystalline basement of the Moesian Platform
4	10	10	Crust-upper mantle transition zone
5	500	75	Upper mantle
6	10		Asthenosphere

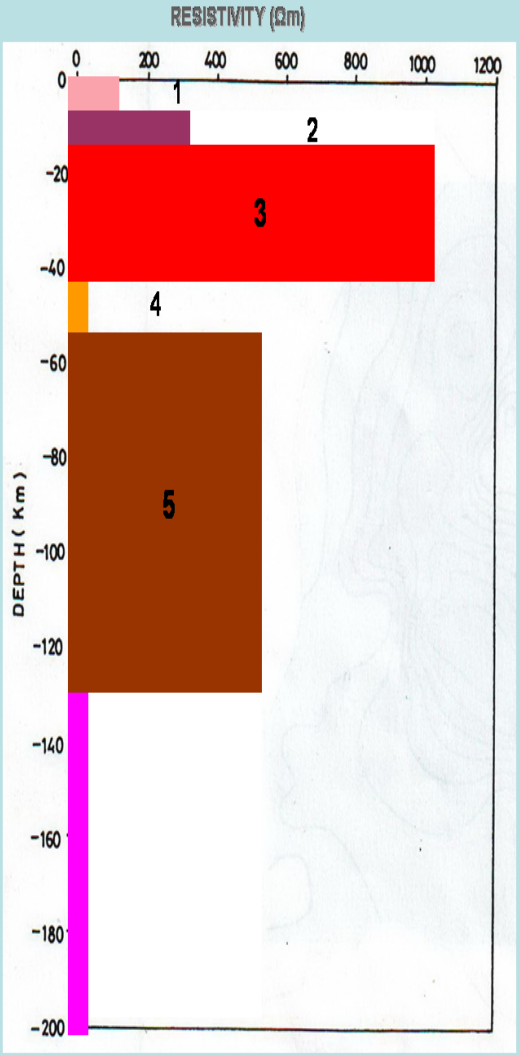

Fig. 2.2.7. MODEL 6: 1-D lithospheric resistivity model for the Southern Carpathians

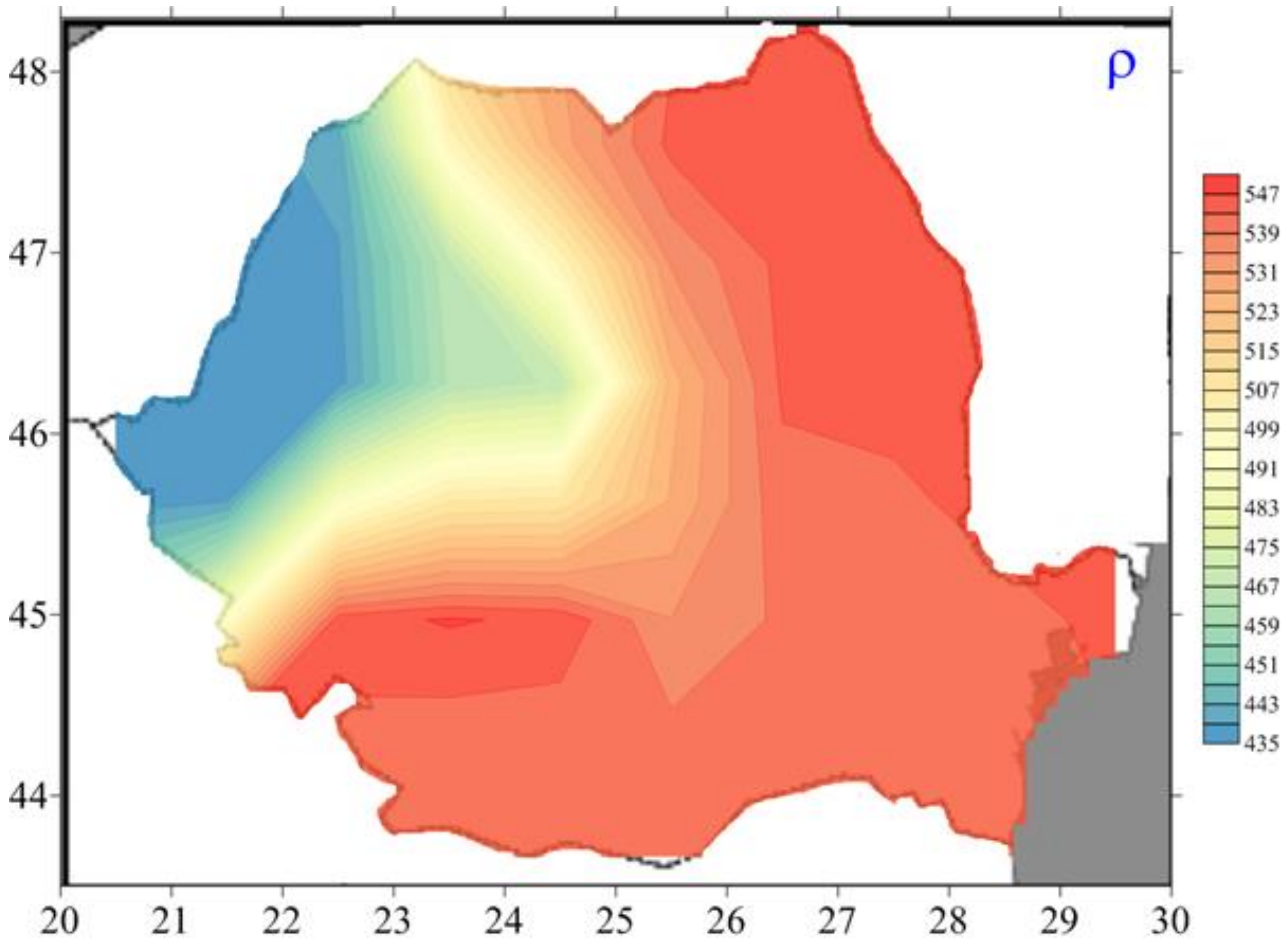

Fig. 2.2.8. The distribution of the crust and upper mantle electric resistivity, based on magneto-telluric data

Chapter III. Analysis of solar eruptive processes and of solar wind, responsible for the moderate geomagnetic activity (geomagnetic storms with minimum Dst between -50 nT and -150 nT) during solar cycle 23

The supersonic magnetised plasma of the solar wind transports a significant quantity of energy (kinetic and magnetic) which, by various physical mechanisms (reconnections, shock waves, etc) is partially transmitted in the terrestrial system magnetosphere – high atmosphere, inducing a series of perturbations in the near-Earth space: geomagnetic storms, substorms, density and the height of radiation belts variability, polar auroras. These disturbances present a similar variability to solar activity phenomena. The geomagnetic perturbations level is well correlated with the speed of the solar wind, especially with the speed of high speed solar streams (HSS). The sectorial magnetic structure of the heliosphere (interplanetary space), with positive and negative polarity sectors, divided by sectorial boundaries, also affects the geomagnetic activity, although, the energy density of the magnetic field is much lower than the one of the solar wind, but, the southern component (negative) of the interplanetary magnetic field sets optimal conditions for the reconnections between the solar wind and the terrestrial system magnetosphere – ionosphere.

Solar wind is the output of the permanent expansion in the heliosphere of the solar corona. The particle flux that composes the solar wind plasma consists of: slow solar wind, characterised by mean velocities of ~400 km/s, continuously emitted, and fast solar wind, with much higher speeds, of ~1000 km/s, emitted by coronal holes that are developing especially in the descending phase of a solar cycle.

Solar cycle 23 started in May 1996 and lasted 12.5 years (until December 2008). The relative sunspot number at maximum places it amongst the low intensity cycles (comparable to SC20, the maximum of 1969). However, if we consider other indices for evaluating the solar cycle intensity, we cannot speak of a low intensity cycle. Thus, considering the total solar irradiance variation, strong flares, fast solar wind parameters, solar cycle 23 is comparable to SC21 and 22 which were much more intense in respect to the relative sunspot number. We notice that during a solar cycle one can distinguish four phases characterised by different properties (Maris et al., 2012), such as:

- The minimum activity phase, apparently a quiet Sun during which the old cycle (the old dipole) consumes its resources manifesting by lower and lower activity at the surface and in the solar atmosphere, but in tachocline (a thin layer at the

bottom the convective layer) the new cycle amplifies its new created dipole and starts its activity at surface through small active regions, with an inverse distribution of the magnetic polarities;

- The ascending phase represents the only interval of a cycle in which the influence of the preceding and following cycles does not manifest itself, through their dipoles;

- The maximum phase is characterised by a significant activity of majority non-stationary solar phenomena, over which is partially superimposed (in the second part) the beginning of the magnetic polarity inversion of the solar dipole (of the magnetic field at poles);

- The descending phase, is the most complex when in the solar atmosphere and in the tachocline two dipoles with magnetic polarities inverted manifest

The durations of the mentioned phases are not unique, rigid, they vary from cycle to cycle, as well as the "classical" duration of a solar cycle. The latter can vary from less than 10 years to over 12-13 years. Table 3.1 shows the duration of solar cycle 20 – 23 phases.

Tabelul 3.1. 11 years solar cycle phases for cycles 20 – 23

SC	Minimum Phase	Ascending Phase	Maximum Phase	Descending Phase
20	01.1964-10.1965	11.1965-11.1967	12.1967 -08.1970	09.1970–05.1975
21	04.1975-02.1977	03.1977-02.1979	03.1979 -12.1981	01.1982–01.1985
22	02.1985-02.1987	03.1987-11.1988	12.1988 -11.1991	12.1991–08.1995
23	09.1995–02.1997	03.1997-08.1999	09.1999-07.2002	08.2002–02.2006

In the following we will discuss the effect of the eruptive solar processes (coronal mass ejections - CMEs) and those of the high speed solar streams (HSS) on the magnetosphere, from the perspective of the hazardeous geomagnetic activity produced by the moderate storms (-150 nT < Dst < -50 nT) from solar cycle 23. We recall that in the 2014 phase of the contract we studied the effects of the intense geomagnetic storms (Dst < -150 nT) during solar cycle 23.

3.1. Analysis of the solar eruptive processes

3.1.1. Event Selection

The main eruptive process whose consequences can be felt on Earth is the coronal mass ejection. A usual ejection can throw out plasma into the interplanetary space, with speeds between 200 and 3000 km/s and its kinetic energy can reach up to orders of 10^{32} ergs

(Zhao and Dryer, 2014). These ejections can produce non-recurrent geomagnetic storms when hitting Earth's magnetic field, given that they contain a strong and constant southward magnetic component (Gosling et al., 1991). On the other hand, fast ejections can trigger a shock in the interplanetary space that plays an important role in generating events with solar energetic particles (SEPs) (Gopalswamy et al., 2003, Cliver and Ling, 2009).

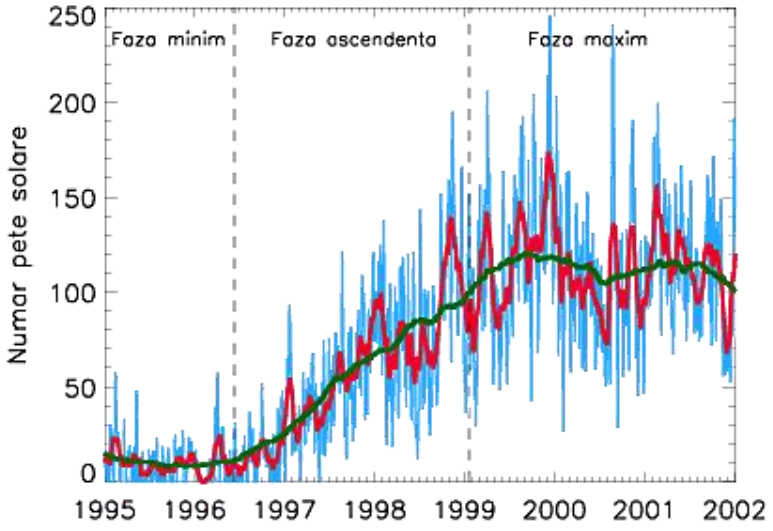

Fig. 3.1.1. The Evolution of the first three phases in solar cycle 23

In this stage of the contract we have analysed the phenomena which took place during the minimum, ascending and maximum phases of the solar cycle 23. There have been 97 geomagnetic storms recorded throughout the minimum, ascending and maximum phases of that solar cycle. These storms were triggered by interplanetary coronal mass ejections, of which 61 have been associated with coronal mass ejections. In this section we analyse those 61 events for which there is a clear association between the geomagnetic storm, the interplanetary coronal mass ejection and the coronal mass ejection. For the identification of this set of events we used the Richardson & Cane (2010) catalogue (available and updated on-line) as well as data from LASCO (Large Angle and Spectrometric Coronagraph) instrument catalogue (http://cdaw.gsfc.nasa.gov/CME_list/) of coronal mass ejections. The LASCO catalogue is based on data provided by the SOHO (Solar and Heliospheric Observatory) mission, namely on white light images from LASCO instrument (Brueckner et al. 1995), on IMP 8, Geotail, Wind and ACE data supplied through OMNIWEB interface (http://cdaw.gsfc.nasa.gov/CME_list/) managed by Goddard Space Flight Center – NASA, and on final data of Dst index values given by the University of Kyoto.

Table 3.2 contains characteristic quantities of the 56 coronal mass ejections selected for this study, such as: date and hour at which the ejection was detected by LASCO, source position on the solar disk, linear speed, speed at the final height of the ejection, the speed at 20 solar radii (~$1.39*10^7$ km), acceleration, as well as the speed at which the interplanetary ejection was recorded at 1 astronomical unit ($1.49*10^8$ km). The coronal mass ejections from Table 1 are mostly Halo (angular width greater than 120°), as seen in LASCO/SOHO white light images.

We studied the evolution of ejections speed in the interplanetary space. The speeds of 27 coronal mass ejections increase in value from 20 solar radii to 1 astronomical unit, which represents 48%, percent which differs from its equivalent for coronal mass ejections that generated major geomagnetic storms – below 25%. The rest of 52% of ejections were decelerated by the interaction with the solar wind. About half of the selected events (25 CMEs) are decelerated after the moment of extrusion from the vicinity of the Sun, a similar result to the one obtained for the CMEs that triggered intense geomagnetic storms. In order to determine the accelerations more precisely and for a more comprehensive study of their variations in time and height and evolution, data from the lower corona is needed. St.Cyr et al. (1999) and J. Zhang et al. (2001) showed that the acceleration is greatest in lower corona and that there is no deceleration below 3 solar radii, despite gravity. 30% of the ejections observed by LASCO/SOHO are decelerated.

The source of coronal ejections can be enframed in a rectangle delimited by longitudes from -35 to 72 and by latitudes from 23 to -22, a narrower rectangle than the one obtained in a previous study (stage 2014 of the contract) that considered the ejections connected to intense geomagnetic storms.

In April 2001 the coronal mass ejection with the highest speeds occurred: 2505 km/s linear speed and 2827 km/s the speed at final height. The transit speed associated to this event was 1020 km/s, which is not the greatest value from the considered events. The greatest transit speed was 1323 km/s associated to the event of May 22, 2002.

Table 3.2: General characteristics of the geo-effective coronal mass ejections

Nr. Crt.	CME	Position	V_{liniar} (km/s)	$V_{Second\ orded}$ at the final height(km/s)	$V_{Second\ orded}$ at 20 Rs (km/s)	Accele-ration (m/s^2)	$V_{tranzit}$ 1 Au (km/s)
	06 jan 1997 – 15:10	S18E06	136	224	319	4.1	507
	07 feb 1997 – 00:30	S38W31	490	718	635	14.3	683

	07 apr 1997 – 14:27	S28E19	878	905	896	3.3	552
	12 may 1997 – 05:30	N21W08	464	335	220	-15	616
	21 may 1997 – 21:00	N05W10	296	322	323	1.4	381
	30 aug 1997 – 01:30	N30E17	371	460	551	9.3	405
	28 sep 1997 – 01:08	N35E10	359	404	409	2.8	580
	6 oct 1997 – 15:28	N30E00	293	524	620	15.9	430
	23 oct 1997 – 11:26	S14W33	503	573	526	3.7	572
	04 nov 1997 – 06:10	S14W33	785	548	698	-22.1	640
	6 dec 1997 – 10:27	--	397	567	525	9	460
	26 dec 1997 – 02:31	--	197	276	378	5.5	430
	02 jan 1998 – 23:28	N24W42	438	548	515	6.5	480
	25 jan 1998 – 15:26	N21E25	693	611	657	-7.4	557
	14 feb 1998 – 06:55	--	123	138	166	0.7	602
	29 apr 1998 – 16:58	S18E20	1374	1151	1250	-44.8	780
	15 oct 1998 – 10:04	N22W01	262	322	321	3.2	510
	04 nov 1998 – 07:54	N17W01	523	723	758	19.6	570
	05 nov 1998 – 20:44	N22W18	1118	949	1044	-24	740
	09 nov 1998 – 18:18	N23W13	325	348	391	2.6	520
	13 apr 1999 – 03:30	N20W00	291	293	298	0.2	520
	28 jul 1999 – 09:06	S15E10	462	443	436	-1.9	710
	17 aug 1999 – 13:31	N23E27	776	1316	1100	45.7	510
	18 jan 2000 – 17:54	S19E11	739	665	697	-7.1	530
	10 feb 2000 – 02:30	N31E04	944	1003	983	11.4	915
	12 feb 2000 – 04:31	N26W23	1107	1047	1086	-8.3	815
	13 may 2000 – 12:26	--	666	755	723	12.8	500
	21 may 2000 – 07:26	--	629	490	327	-20.1	650
	06 jun 2000 – 15:54	N20E18	1119	1130	1125	1.5	1007
	12 jul 2000 – 20:30	N15W70	820	789	810	-3.2	965
	17 jul 2000 – 08:54	S10E45	788	1060	1025	30.7	--
	25 jul 2000 – 03:30	N06W08	528	494	425	-5.8	550
	06 aug 2000 – 18:30	N10E30	233	475	444	8.5	510
	09 oct 2000 – 23:50	N01W14	798	709	747	-9.8	590
	25 oct 2000 – 08:26	N09W63	770	948	885	17.4	565
	24 nov 2000 – 05:30	N21W07	1289	1298	1296	2.1	--
	18 dec 2000 – 11:50	N15E01	510	372	0	-26.8	380
	20 jan 2001 – 21:30	S07E46	1507	1264	1437	-41.1	680
	28 feb 2001 – 14:50	--	313	345	356	1.9	610
	16 mar 2001 – 03:50	--	271	362	317	2.6	520
	25 mar 2001 – 17:06	N16E25	677	522	600	-12.2	850
	02 apr 2001 – 22:06	N15W60	2505	2827	2634	108.5	1020
	06 apr 2001 – 19:30	S21E31	1270	914	1215	-57.3	1050

	11 apr 2001 – 13:31	S22W27	1103	1019	1065	-13	990
	14 aug 2001 – 16:01	N16W36	618	601	625	-4.8	620
	20 sep 2001 – 19:31	--	446	404	403	-3.4	570
	27 sep 2001 – 04:54	S20W30	509	1109	929	36.6	790
	28 sep 2001 – 08:54	N10E18	846	785	807	-6.9	710
	29 sep 2001 – 11:54	N15E05	509	470	150	-12	715
	26 dec 2001 – 05:30	N10W60	1446	1284	1295	-39.9	580
	20 mar 2002 – 17:54	S17W20	603	501	344	-15.8	625
	15 apr 2002 – 03:50	S15W01	720	742	731	2.1	750
	17 apr 2002 – 08:26	S14W34	1240	1103	1198	-19.8	863
	08 may 2002 – 13:50	S12W07	614	697	1468	78.9	610
	22 may 2002 – 03:50	S30W34	1557	1504	1540	-10.4	1323
	29 jul 2002 – 12:07	S10W10	222	309	305	3.3	500

3.1.2. Correlation analysis

As the geomagnetic storms are characterised by the minimum value of the Dst index, in the present study we analysed possible correlations for the selected events. Figures 3.1.2 and 3.1.3 show the variation of the CME linear speed with respect to the Dst index, for the intervals of minimum and ascending phases of solar cycle 23 (September 1995 - August 1999) and, maximum phase respectively, (September 1999 - August 2002).

On each figure there are shown f(x) – a function with linear regression and R^2 – determination coefficient. In percentage, this coefficient shows how much from the variance of the Dst variable in relationship with the considered variable, is explained by the f(x) equation. For the first interval R^2 is 0, but for the maximum phase is 15%. This percentage has encouraged us to analyse also the correlation between the product V*Bz (linear speed of the coronal mass ejection times the southward component of the interplanetary magnetic field), shown in figures 3.1.4 and 3.1.5, and the Dst index. The determination coefficient for the first considered interval has risen up to 11% and for the second interval it has dropped to 8%.

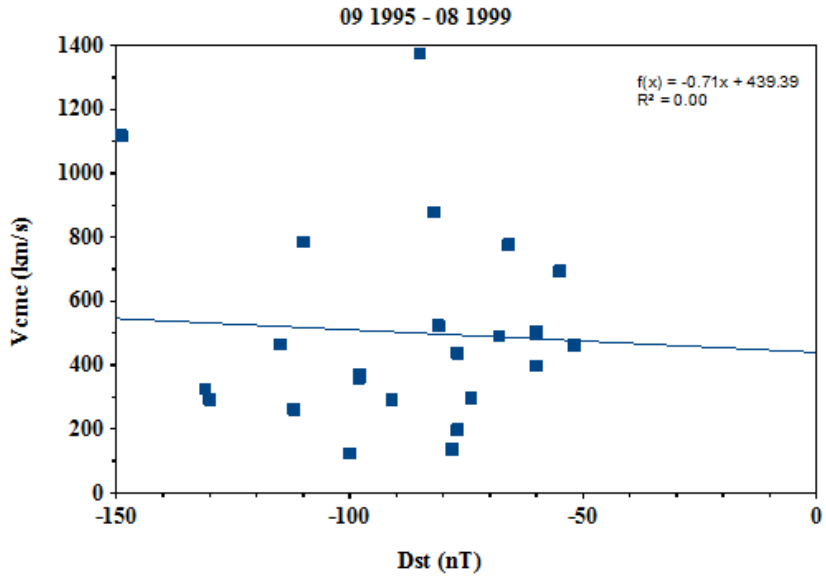

Fig. 3.1.2. Dst variation as a function of f coronal mass ejections speed during minimum and ascending phases of the solar cycle 23

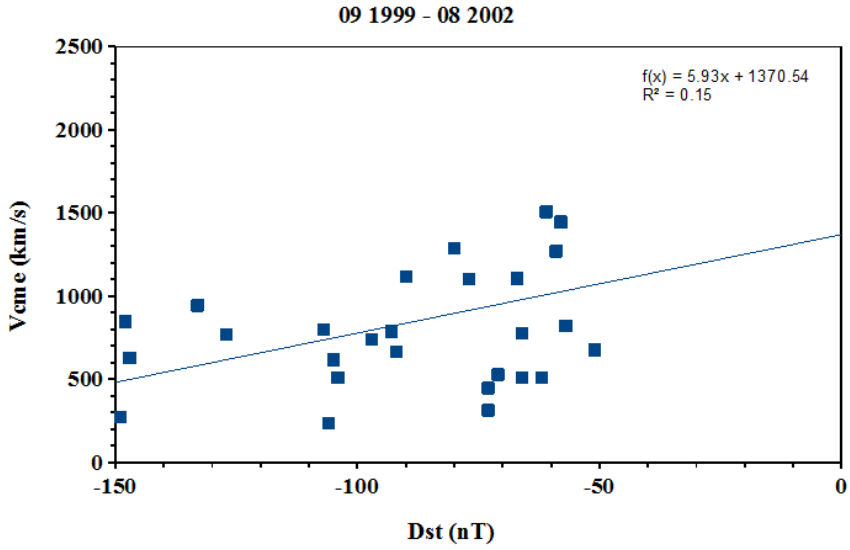

Fig. 3.1.3. Dst variation as a function of coronal mass ejections speed during maximum phase of the solar cycle 23

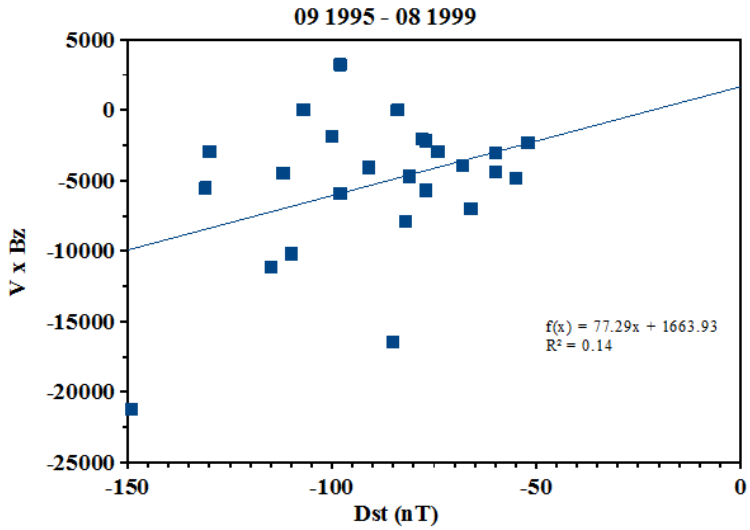

Fig. 3.1.4. Dst variation as a function of the product between coronal mass ejections speed and the minimum value of the Bz component of the interplanetary magnetic field during minimum and ascending phases of the solar cycle 23

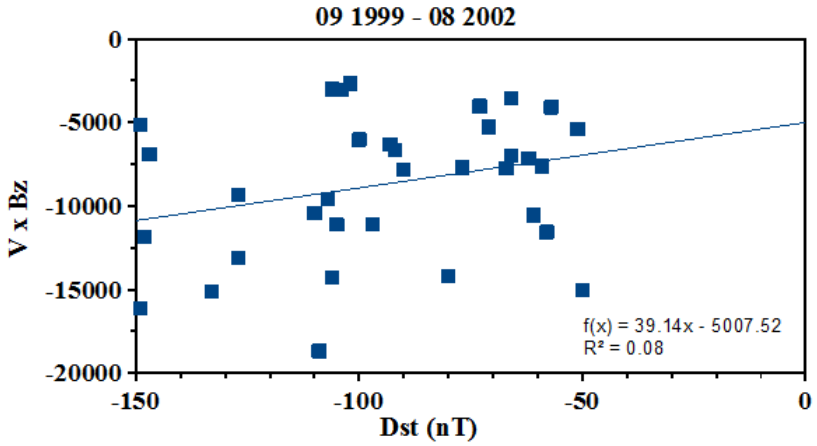

Fig. 3.1.5. Dst variation as a function of the product between coronal mass ejections speed and the minimum value of the Bz component of the interplanetary magnetic field during maximum phase of the solar cycle 23

The analysis of the Dst values dispersion in relationship with the product V*Bz suggests that the geomagnetic efficiency needs to take in account this product.

Another correlation that we studied was the dispersion between the kinetic energy of coronal ejections and the minimum value of Dst. The coronal mass ejections LASCO catalogue in some cases estimates the mass of the ejected plasma and calculates the kinetic

energy starting from this mass and from the recorded linear speed. Figures 3.1.6 and 3.1.7 present the plots of this variation. It can be seen that the value of the determination coefficient is 0.02 for the events during the minimum and ascending periods of solar cycle 23, and 0.11 for the events during the maximum solar activity period from this cycle.

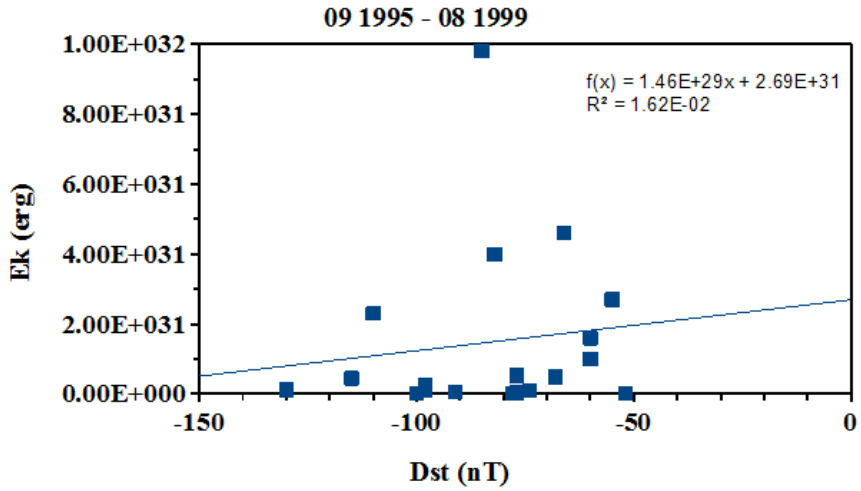

Fig. 3.1.6. Dst variation as a function of coronal mass ejection kinetic energy during minimum and ascending phases of the solar cycle 23

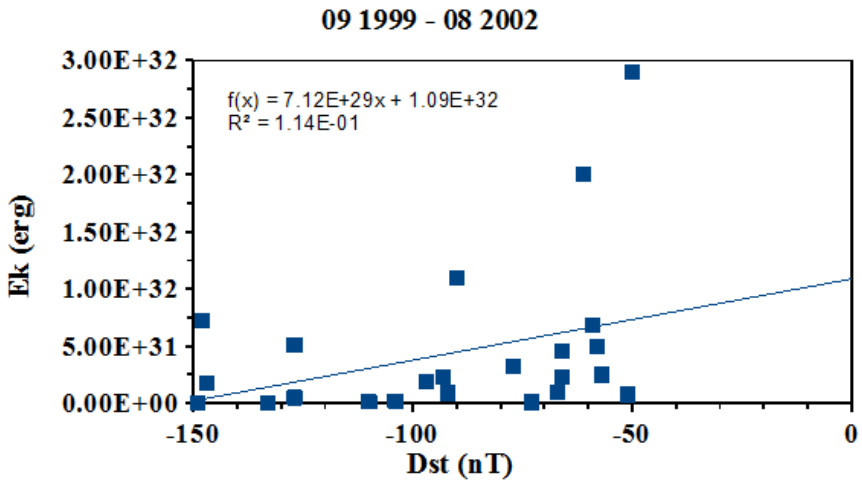

Fig. 3.1.7. Dst variation as a function of coronal mass ejection kinetic energy during maximum phase of the solar cycle 23

3.2. Fast solar wind analysis

For detailed analysis of the relationship between the high speed solar streams in solar wind (HSS) and their effects in the magnetosphere (geomagnetic storms) one needs the available data processed in various phases of the cycle. Thus one can emphasise various

characteristics and/or parameters that can be taken into account in order to empirically model the efficiency that HSS produces geomagnetic storms (GS).

In the present study we established HSS that have produced GS of moderate intensity (-150 nT< Dst < -50 nT) in the magnetosphere and we showed by means of correlation analysis the HSS and the IMF (interplanetary magnetic field) parameters that have influence over the intensity of the geomagnetic storms measured by the Dst index.

3.2.1. HSS and geomagnetic storms

Solar wind, continuum plasma flux from the solar corona, is an inhomogeneous medium structured by various parameters (density, plasma speed, heliospheric magnetic field structure) and because of this it is hard to forecast its behaviour in the near-Earth space. However, some of its structures, emitted and controlled by their solar sources, can be forecasted with sufficient precision (between 70-95%). Thus, HSSs with the origin in coronal holes (CH) represent a repetitive structure that lasts several solar rotations and thus possible to forecast. Their geoeffectivity is directly dependant on the solar source (CH), being influenced by their heliographic position and their morphological structure. Therefore, CH from the equatorial zone or with large extensions towards the equator (observed especially in the minimum solar activity years or the end of the descending phase) produce HSS with a major effect in the magnetosphere.

For the present study we used two catalogues elaborated during the HELIOTRER (2007 – 2010) project (Mariș & Mariș, 2010; Mariș & Mariș, 2012). The high speed solar streams for the minimum, ascending and maximum phases of the solar cycle 23, are shown in Table 3.3. The first three columns of this table show the specific date (year, month, day) when the HSS started, column 4 – V0, the initial speed of the solar wind in the day that the HSS started, column 5 – Vmax, the maximum speed of the HSS, column 6 – the duration in days , column 7 - **ΔVmax = Vmax – V0**, the velocity gradient of the HSS. The next two columns specify the minimum value of the southern component (Bz, nT) of the interplanetary magnetic field, forgoing the minimum value of the Dst, and the moment of its recording by month, day and hour. The last two columns specify the minimum Dst (nT) and the moment of its recording.

Table 3.3. HSS and geomagnetic storms of medium intensity during the minimum, ascending and descending phases of the SC23

Year	Month	Day	V0	Vmax	Dur	ΔVmax	Bz min.	t (Bz min.)	Dst_min.	t (Dst min.)
			km/s	km/s	days	km/s	nT	mm:zz:hh	nT	mm:zz:hh
HSS							IMF		FG	
MINIMUM PHASE										
1996	3	9	320,3	571,7	7,2	251,4	-8,3	03:11:01	-60	03:11:03
1996	3	19	379,7	643,7	5	264	-5,3	03:20:21	-54	03:20:23
1996	3	24	423	577,7	3,9	154,7	-7,3	03:24:23	-60	03:25:01
1996	4	13	392,7	604,3	3,1	211,6	-7,2	04:14:22	-56	04:15:00
1996	4	16	438,3	714,7	5,9	276,4	-3,9	04:17:06	-52	04:17:08
1996	9	9	348	665,7	9,4	317,7	-4,1	09:12:07	-54	09:12:08
1996	9	19	454,3	656,3	5,4	202	-3,2	09:23:06	-51	09:23:07
1996	9	25	411,3	636,7	4,5	225,4	-3,9	09:26:21	-50	09:27:00
1996	10	17	371,7	619,3	4,9	247,6	-5,4	10:19:14	-52	10:19:16
1996	10	21	406,3	642	4	235,7	-9,7	10:23:02	-105	10:23:04
ASCENDING PHASE										
1997	3	24	350	576,3	7,6	226,3	-7,5	03:28:19	-63	03:28:23
1997	4	16	310	541,3	6,9	231,3	-9,3	04:17:04	-77	04:17:05
1997	9	30	373,3	486,4	3,8	113,1	-9,4	10:01:12	-98	10:01:15
1997	10	23	314,7	539	8,6	224,3	-9,2	10:25:00	-64	10:25:02
1998	1	19	303,3	467,7	12,1	164,4	-7,2	01:30:10	-55	01:30:11
1998	3	9	267,7	543,7	7,4	276	-15	03:10:16	-116	03:10:20
1998	3	20	312,3	601,3	4,8	289	-12,6	03:21:13	-85	03:21:15
1998	3	25	356	491,7	7,9	135,7	-6,7	03:29:17	-54	03:29:19
1998	4	23	322,7	491,3	6,2	168,6	-9,1	04:24:04	-69	04:24:07
1998	4	23	322,7	491,3	6,2	168,6	-7,6	04:26:13	-63	04:26:17
1998	4	30	318,3	641	3,4	322,7	-11,8	05:02:13	-85	05:02:17
1998	6	6	369,7	623	5,6	253,3	-9,6	06:06:19	-50	06:06:21
1998	7	15	305	602	5,2	297	-3,3	07:16:14	-58	07:16:16
1998	10	7	345,3	583	5,2	237,7	-11,4	10:07:17	-70	10:07:22
1998	12	24	324,3	517,3	4	193	-10	12:25:09	-57	12:25:11
1999	2	28	339	529,7	3,8	190,7	-14,4	03:01:15	-95	03:01:19
1999	3	3	405,3	573,3	5,4	168	-7,1	03:07:05	-57	03:07:10
1999	3	29	325,7	532,3	4,1	206,7	-11,1	03:29:12	-56	03:29:14
MAXIMUM PHASE										
1999	9	9	397	609,3	10,4	212,3	-6,3	09:13:00	-74	09:13:04
1999	9	22	355,7	595	4	239,3	-15	09:22:20	-173	09:22:23
1999	9	26	354,7	632,7	7,8	278	-5,9	09:27:14	-64	09:27:18
1999	9	26	354,7	632,7	7,8	278	-5,6	09:30:01	-61	09:30:03
1999	10	9	388	710,7	9,6	322,7	-9	10:10:15	-67	10:10:18
1999	10	9	388	710,7	9,6	322,7	-5,7	10:13:16	-60	10:13:17
1999	10	9	388	710,7	9,6	322,7	-5,1	10:14:23	-67	10:15:05
1999	10	20	328	670,7	7,6	342,7	-30,7	10:22:05	-237	10:22:06
1999	11	6	335	662,7	9,3	327,7	-7,2	11:08:12	-73	11:08:14
1999	11	16	314,7	582,7	5,4	268	-11,6	11:16:12	-79	11:16:16
1999	12	29	349	744,7	11	395,7	-2,9	12:31:22	-50	12:31:23
2000	1	10	320	597	8	277	-15,1	01:11:20	-81	01:11:21
2000	3	5	315,7	467,3	6,4	151,6	-6,6	03:08:19	-51	03:08:21
2000	5	29	337,7	637,3	5,1	299,7	-8,9	05:29:16	-54	05:29:21
2000	8	4	427,7	566,3	3,9	138,6	-3,7	08:06:03	-56	08:06:05
2000	8	27	354,3	610	7,3	255,7	-4,6	08:29:05	-60	08:29:06
2000	8	27	354,3	610	7,3	255,7	-6,6	09:02:08	-57	09:02:14
2000	9	24	385,7	584	5	198,3	-5,6	09:26:00	-55	09:26:02
2000	10	22	360,3	556,3	4,8	196	-4,8	10:23:05	-53	10:23:07

2001	3	22	291	438	4,8	147	-7,5	03:23:14	-75	03:23:16
2001	6	18	292,3	765,7	11,6	473,4	-11,8	06:18:06	-61	06:18:08
2002	1	9	344,7	639	8,5	294,3	-4,5	01:11:04	-72	01:11:06
2002	2	4	322,3	661,3	6,2	339	-7,7	02:05:19	-82	02:05:20
2002	5	26	429,7	749	4,6	319,3	-12	05:27:07	-64	05:27:08

From Table 3.3. one can see that for most of the cases, the time of the Bz min registration precedes the one for Dst min by 2 hours, there are only two cases with six hours, two cases with five, and one for which the two minima coincide. By analysing the main phases of all the geomagnetic storms one can notice the negative values of the Bz throughout the main phase, with very little exceptions when Bz had one positive value. This fact proves the existence of the necessary condition ($Bz < 0$) in order to have the reconnection of the terrestrial magnetic field lines with those belonging to the interplanetary magnetic field, thus assuring the transfer of energy from the solar wind into the magnetosphere, in front of the magnetosphere.

By comparing the number of HSS produced by CH that triggered moderate geomagnetic storms, one notices the large number of event in the maximum phase (24) compared to the minimum phase of the solar cycle 23 (only 10 events).

3.2.2. Correlation analysis

Considering the fact that the geomagnetic storm intensity is determined by the energy transferred from HSS to the magnetosphere, which in its turn depends on the HSS parameters and on Bz, we analysed their degree of linear dependence by means of correlation analysis. Fig. 3.2.1 llustrates the distribution of Dst values depending on the HSS parameters, Vmax (upper left side) and ΔVmax (upper right side), for the minimum phase of the solar cycle 23. The values of the determination coefficients obtained show that the percent in which Dst is influenced by the maximum speed or by the speed gradient of the triggering HSS, is 1%.

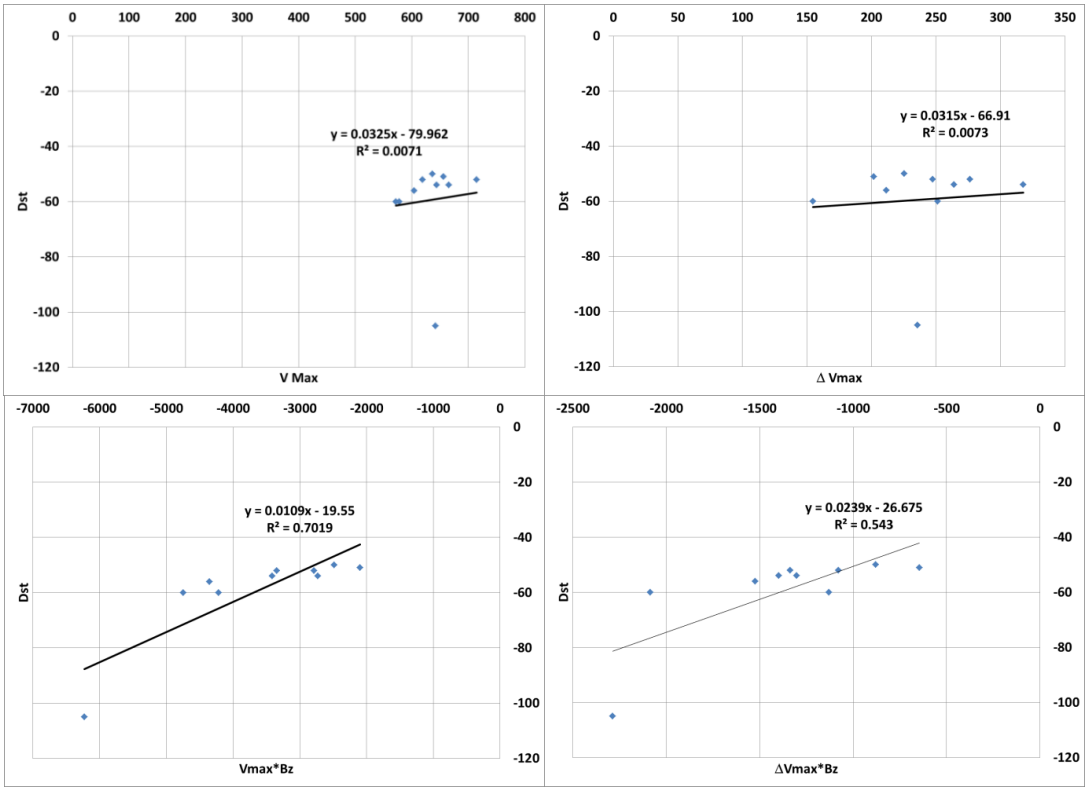

Fig. 3.2.1. Dst variation as a function of HSS parameters in the minimum phase of solar cycle 23

The correlation analysis of Dst with the product (Vmax*Bz) and with the product (ΔVmax*Bz) reveals the importance of the southward component of the IMF (Bz), which grows up to 70%, 54 % respectively, the combined contribution of the maximum speed of the HSS and of the component Bz (Fig. 3.2.1. lower right and left frames, respectively).

The results of correlation analysis for the ascending phase of cycle 23 are presented in figure 3.2.2. It can be easily seen in the lower frames of Fig. 3.2.2 the significant growth of the determination factor for the cases in which the combined effect of the HSS speed and of the southward component of IMF is considered. On notices the lower values of the determination factor while considering the combined effect of HSS and IMF on Dst variation, in the ascending phase of the cycle, unlike the ones in the minimum phase.

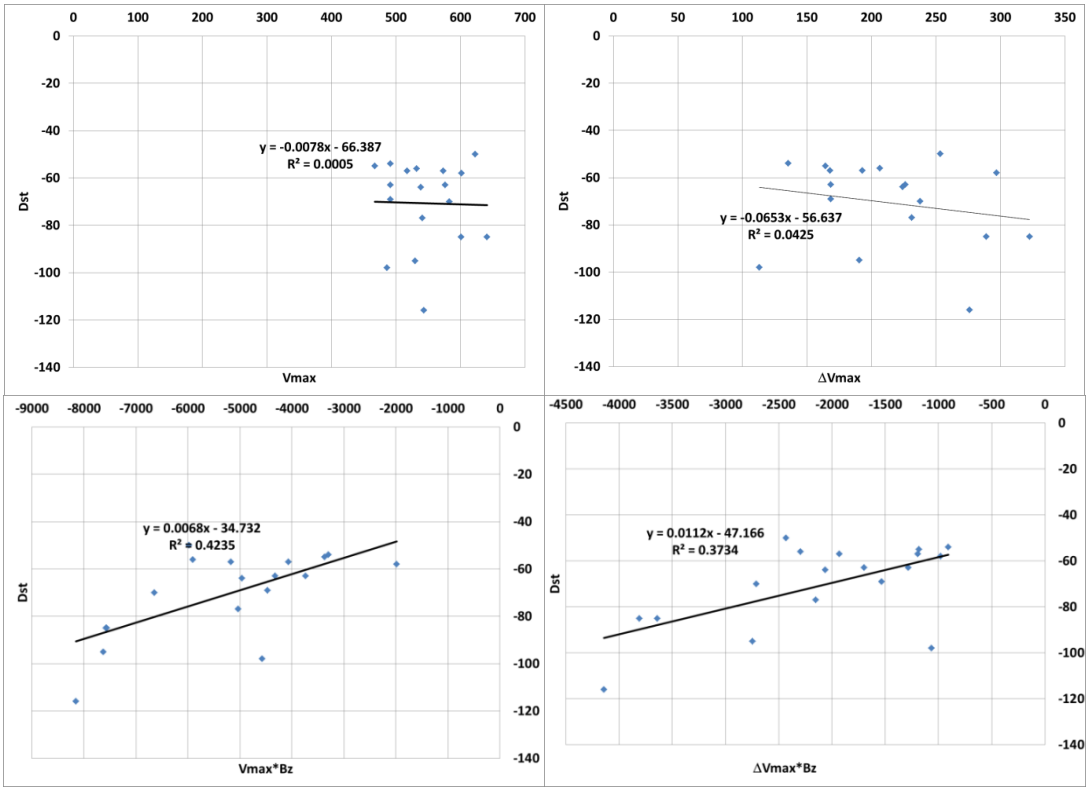

Fig 3.2.2. Dst variation as a function of HSS parameters in the ascending phase of solar cycle 23

The correlation analysis results for the maximum phase of the cycle are presented in figure 3.2.3. In order to easily follow the determination coefficient variation, we set up the obtained values in Table 3.4 for all the considered phases of the cycle 23.

Table 3.4. The determination coefficient (R^2) of the maximum speed of HSS and Bz over the Dst variation in different phases of the cycle 23

Phase of cycle 23	**(Vmax, Dst)**	**(Vmax*Bz, Dst)**	**(ΔVmax, Dst)**	**(ΔVmax*Bz, Dst)**
Minim	0,0071	**0,7019**	0,0073	**0,5430**
Ascendentă	0,0005	**0,4235**	0,0425	**0,3734**
Maxim	0,0010	**0,7013**	0,0135	**0,6219**

For all the three analysed phases of the solar cycle 23, in Table 3.3 it can be seen that the effect of the maximum speed and of the speed gradient of HSS is practically absent in Dst variation (R^2 values between 0,001 and 0,0425). The combined effect of HSS speed and of the southward component of IMF (Bz) is determining for the Dst variation in all the analysed phases. One emphasizes the highest values of R^2 in maximum phase of the cycle, values close to these ones during he minimum phase, while for the ascending phase the weakest determination was obtained. Also, it can be noticed the high values of R^2 for the

combined effect of Vmax*Bz in comparison to the effect of the product ΔVmax*Bz in Dst variation.

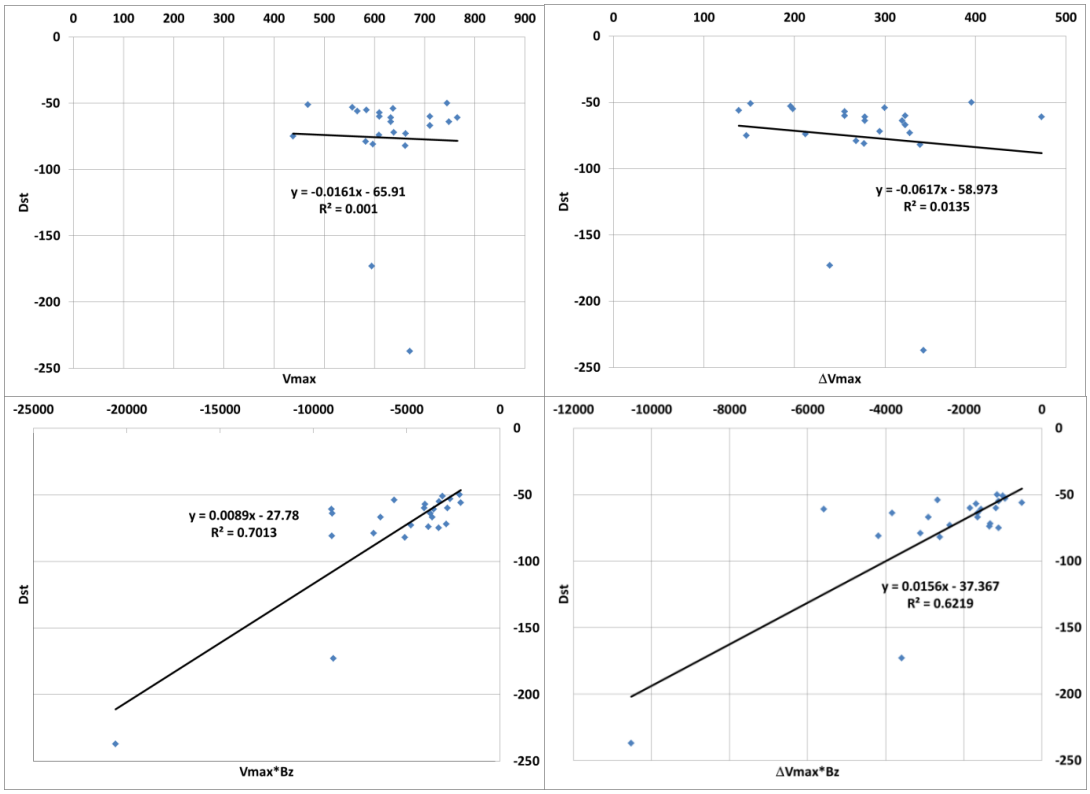

Fig. 3.2.3. Dst variation as a function of HSS parameters in the maximum phase of solar cycle 23

3.2.3. Conclusions and future objectives

From the analysis carried out for the first three phases of the solar cycle 23 we conclude the following:

- The Dst variation that determines the geomagnetic storm intensity is determined to a large extent by the southern component Bz of the interplanetary magnetic field, than the variation and the magnitude of the speed of the high speed solar stream from the solar wind that contributes to triggering the storm;
- The time delay between the minimum values of Bz and Dst (2 – 6 hours) allows the real time forecast of the geomagnetic ongoing storm intensity;
- The determination degree of the Dst variation as a function of the HSS and IMF parameters is lower on the ascending phase, which will decrease the degree of confidence in the foreseen geomagnetic storm intensity.

The present study will continue with a similar analysis for the descending phase of solar cycle 23 and a study of the coronal holes, sources of HSS, for each phase of the cycle. Based on obtained results, an empirical method of forecasting the geoeficiency of the HSS will be elaborated.

3.3. Modelling the geomagnetic efficiency

Modelling the geomagnetic efficiency of some eruptive solar processes implies setting some cause and effect relationships between some characteristic quantities of the analysed phenomena. In this study we are referring to the coronal mass ejection, or the high speed stream, and the triggering of a moderate geomagnetic storm. We chose the index Dst as a characteristic parameter of the geomagnetic storm.

The coronal mass ejection that produced the most powerful geomagnetic storm from the presented selection was on April 17, 2002, a halo ejection, with linear speed of 1240 km/s and therefore a rapid ejection. On the other side, the least efficient ejection is also the most rapid from the selection, from April 2nd, 2001, with a linear speed of 2505 km/s. The first ejection's source is S14W34, and the second one's is N15W60, thus confirming recent studies (Zhang et al. 2007) regarding the efficiency of ejections as a function of their position, which is: the high latitude sources are less probable to be geo-effective due to the propagation at higher latitudes in the heliosphere and thus not intercepting the Earth.

The efficiency with which a coronal ejection will manifest itself depends greatly on the interplanetary conditions, as it can be seen in the correlation study of the product V*Bz. Therefore, future studies must include more descriptive parameters of the interplanetary plasma.

References

Brueckner G.E., Howard, R.A., Koomen, M.J., Korendyke, C.M., Michels, D.J., Moses, J.D., Socker, D. G., Dere, K.P., Lamy, P. L., Llebaria, A., Bout, M. V., Schwenn, R., Simnett, G. M., Bedford, D. K., Eyles, C. J. (1995), *The Large Angle Spectroscopic Coronagraph (LASCO)*, Solar Physics, **162** (1-2), 357-402

Cliver, E.W. and Ling, A.G. *Low-frequency type III bursts and solar energetical particles*, Astrophysical Journal, 690, 598-609, 2009

Gosling, J.T., McComas, D.J., Phillips, J.L. And Bame, S.J. *Geomagnetic activity associated with Earth passage of itnerplanetary shock disturbances and coronal mass ejections*, Journal of Geophysical Research, 96, 7831-7839, 1991

Gopalswamy, N, Yashiro, S., Lara, A., Kaise, M.L., Thomson, B.J., Gallagher, P.T. And Howard, R.A. *Large solar energetic particle events of cycle 23: A global overview*, Geophysical Reseach Letters, 30(12), 8015, 2003

Mariş, O., Mariş, G.: 2010, COMPLEX CATALOGUE (GEOMAGNETIC STORMS - HIGH SPEED STREAMS during Solar Cycle 23, 1996 – 2008), (http://www.spacescience.ro/new1/GS_HSS_Catalogue.htm).

G. Maris, O. Maris: High speed streams in the solar wind during the 23rd solar cycle, in: Advances in Solar and Solar-Terrestrial Physics, Editors: G. Maris & C. Demetrescu, Published by Research Signpost 2012; Trivandrum-695 023, Kerala, India, ISBN 978-81-308-0483-5, pp. 97-134.

G. Maris, O. Maris, C. Oprea, M., Mierla: High-speed streams in the solar wind during the last solar minimum, in: Comparative Magnetic Minima: Characterizing quiet times in the Sun and Stars, Proceedings of the International Astronomical Union, IAU Symposium, Volume 286, p. 229-233, DOI: 10.1017/S1743921312004887, 07/2012.

Richardson and Cane:"Near-Earth Interplanetary Coronal Mass Ejections During Solar Cycle 23 (1996--2009): Catalog and Summary of Properties" 2010, Solar Physics

St.Cyr, O.C., Burkepile, J.T., Hundhausen, A.J., Lecinski, A..R. *A comparison of ground-based and spacecraft observations of coronal mass ejections from 1980-1989*, Journal of Geophysical Research, 104, 12493-12506, 1999

Zhang J., Dere, K.P., Howard, R.A., Kundu, M.R., White, S.M. On the Temporal Relationship between Coronal Mass Ejections and Flares, Astrophysical Journal, 559, 452-462, 2001

J. Zhang, I. G. Richardson, D. F.Webb, N. Gopalswamy, E. Huttunen, J. C. Kasper, N. V. Nitta, W. Poomvises, B. J. Thompson, C.-C. Wu, S. Yashiro, and A. N. Zhukov: "Solar and interplanetary sources of major geomagnetic storms (Dst 100 nT) during 1996–2005", Journal of Geophysical Research, 112, A10102, 2007

Zhao X. and Dryer M. *Current status of CME/shock arrival time prediction, Space Weather*, 12, doi:10.1002/2014SW001060, 2014

Chapter IV. Modelling of geophysically induced currents (GIC) by geomagnetic storms produced by solar eruptive phenomena, stage 2015

The interaction of the solar wind and heliospheric magnetic field with the magnetosphere and ionosphere results in variations of the geomagnetic field that induce hazardous electric currents in grounded technological systems (electric power and hydrocarbon transportation networks), the so-called GICs. In order to evaluate the hazard induced on the European continent, we present a study of the surface electric field induced by 16 intense (Dst < -150 nT) geomagnetic storms, based on the analysis of the geomagnetic records from the European network of observatories, study that tend to solve the geophysical part of the problem. In the present stage of the project, we explored the evolution and sources of the disturbance field and of the induced field, during the strongest storm recorded in the solar cycle 23, namely the November 20-21, 2003 one, characterized by a Dst index of -422 nT, as well as the geographical distribution of the maximum surface electric field induced by each of the considered 16 storms of the study.

4.1. Data and method

1-minute values of the northward and eastward geomagnetic elements, recorded at up to 29 European observatories from the INTERMAGNET network during six days encompassing the 16 intense storms of the study (Table 4.1), were processed to get the time derivative that is driving the induced electric field. A computer code worked out during the previous stage of the project, improved during the present stage, have been used for that purpose.

The induced electric field is assessed according to the method of Viljanen and Pirjola (1989), presented in the report for the 2014 stage and shortly reviewed in the next lines.

Generally, the horizontal electric field (Ex, Ey) produced by the variable magnetic field is linked to the magnetic field (Bx, By) through the impedance Z(ω) of the underground subject to the plane wave that approximates the propagation of the geomagnetic disturbance.

$$E_x(\omega) = \frac{Z(\omega)}{\mu_0} B_y(\omega), E_y(\omega) = \frac{Z(\omega)}{\mu_0} B_x(\omega)$$

For an Earth viewed as a halfspace with a conductivity σ, the surface electric field is described by

$$E_y(t) = -\frac{1}{\sqrt{\pi\mu_0\sigma}} \int_{-\infty}^{t} \frac{g_x(u)}{\sqrt{t-u}} du \,,$$

where g_x denotes the time derivative of the field B. The integral is converted to a sum that allows to calculate the 1-minute E values. A numerical code was written for the present study. We mention here that two other methods to estimate the geographical distribution of the induced geoelectric field in a denser network of points are presently in use (Viljanen et al., 2014; Matandirotya et al., 2015).

Table 4.1

Year	Date	Dst (nT)	Year	Date	Dst (nT)
1998	May, 4	-205	2001	Apr, 11	-271
1998	Sep, 25	-207	2001	Nov, 5	-292
1999	Oct, 21	-237	2001	Nov, 24	-221
2000	Apr, 6	-287	2003	Oct, 29	-383
2000	Jul, 15	-301	2003	Nov, 20	-422
2000	Aug, 12	-235	2004	Nov, 7	-374
2000	Sep, 17	-201	2005	May, 15	-247
2001	March, 31	-387	2005	Aug, 24	-184

4.2. Results

The largest storm of the solar cycle 23, namely – November 20-21, 2003, Dst = -422 nT – was produced by the interaction with the magnetosphere of the ICME illustrated in Fig. 1 by parameters of the solar wind recorded at the Lagrangean point 1 and available at http://omniweb.gsfc.nasa.gov/. The total heliospheric magnetic field, B, the Bz component, the density, velocity and dynamic pressure, N, V, and respectively Pw are shown. The evolution of the storm is illustrated in the same figure by means of the Dst geomagnetic index.

To get an idea on the latitudinal differences that characterize the evolution of the geomagnetic field and of its time derivative, as well as of the induced surface geoelectric field during a geomagnetic storm, we show in Fig. 2 the results obtained for a longitudinal chain of observatories along the 105°E geomagnetic meridian. To show the extreme possible variations, the AL geomagnetic index, showing the disturbed field produced by the ionospheric electrojet at auroral latitude, and the Dst index, showing the disturbed field produced by the magnetospheric ring current at the geomagnetic equator, are plotted on top and, respectively, at the figure bottom.

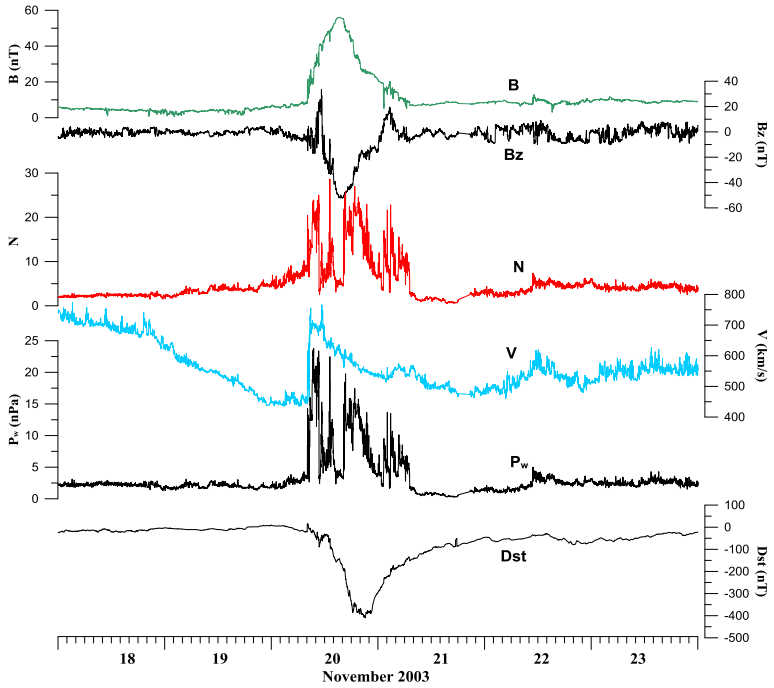

Fig. 4.1. Solar wind parameters and the Dst evolution for the November 2003 storm

Examining the figure several conclusions can be underlined, namely:

- the disturbance in Bx is 2-3 times larger at northern latitudes than at mid and southern latitudes;
- during the geomagnetic storm, effects of auroral electrojets superimpose at all latitudes on the disturbance created by the magetospheric ring current;
- the amplitude of the geoelectric field produced by magnetic variations is of the order of hundreths of mV/km in case of SUA (45°N), and of 1-2 mV/km in case of UPS (60°N);
- the more pronounced geoelectric component is directed East-West.

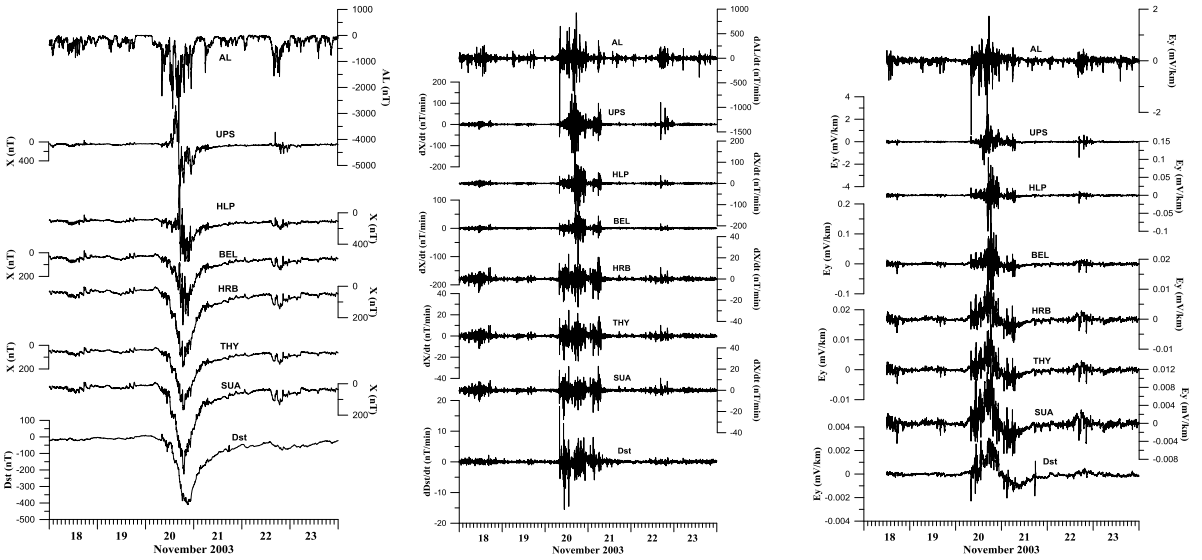

Fig. 4.2. The geomagnetic disturbance (Bx) (left), its time derivative (middle), and the resulting surface electric field (Ey) (right) for the November 2003 storm, at geomagnetic observatories along the 105°E geomagnetic meridian

The surface electric field at the European observatories considered in the present study was calculated for various moments of the storm development in its initial and main phases, marked in Fig. 4.3. In the left panel the evolution of the electric field at a mid-latitude observatory (HRB – Hurbanovo) is presented as an example, and in the right panel the Dst index was plotted. For each of the moments marked in Fig. 4.3 by vertical lines, maps of the surface electric field were drawn, of which we give a few examples in Fig. 4.4.

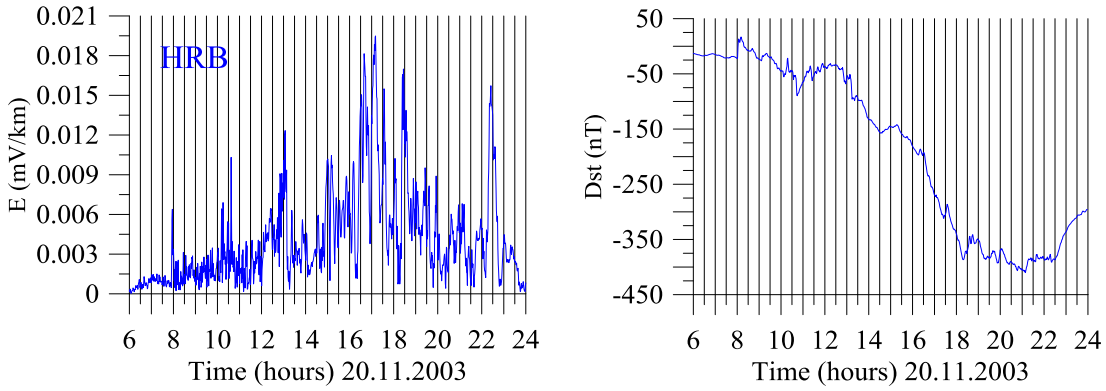

Fig. 4.3. The evolution of the November 2003 geomagnetic storm in its initial and main phases through the surface electric field at HRB (left plot) and Dst index (right plot). Vertical lines indicate moments for which maps of the electric field were drawn

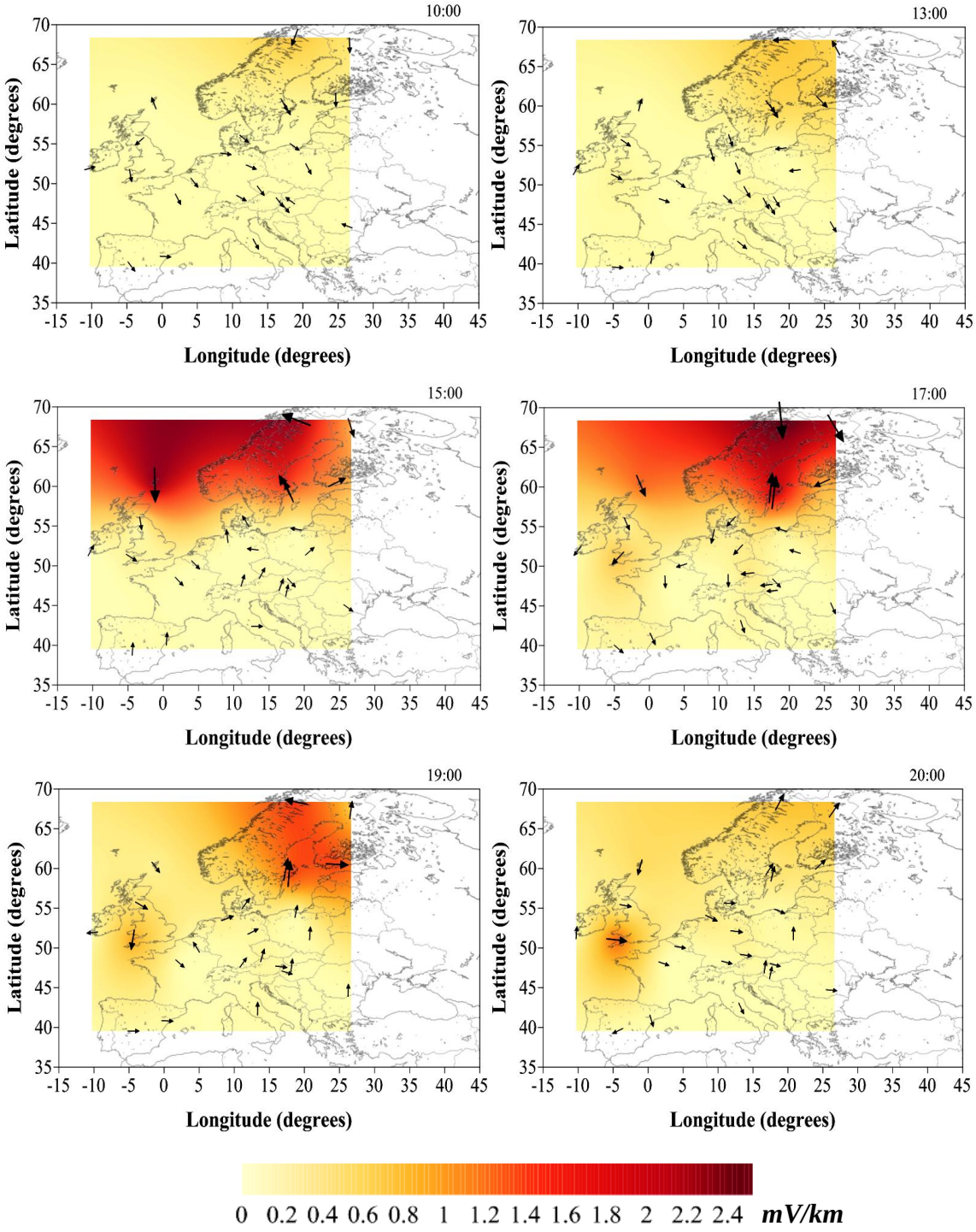

Fig. 4.4. Snapshots of surface electric field maps during the initial and main phases of the November 2003 storm, for moments marked on each map. The orientation of the field is given by arrows, and the magnitude by both colors and arrows length

The maps show that (1) the largest disturbances occur in Scandinavia, and to a lesser extent, in England and Western France, and (2) the direction of the electric field is highly

variable during the storm and is not necessarily the same at all points at a certain moment of the storm.

As regards the sources of the variations observed, our study indicates both the magnetospheric ring current and the ionospheric auroral electrojet. Fig. 4.5 shows the geographical distribution of the correlation coefficient between the observed geomagnetic disturbance and the Dst index, while Fig. 4.6 shows that in case of northern latitude observatories the auroral electrojet and sometimes the magnetopause currents produced by solar wind pressure impulses are a good candidate.

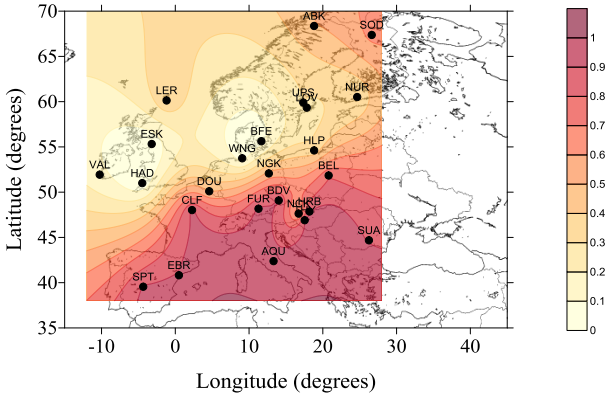

Fig. 4.5. Correlation coefficient between the Dst index and the horizontal component disturbance at European observatories, for the November 20-21, 2003 storm

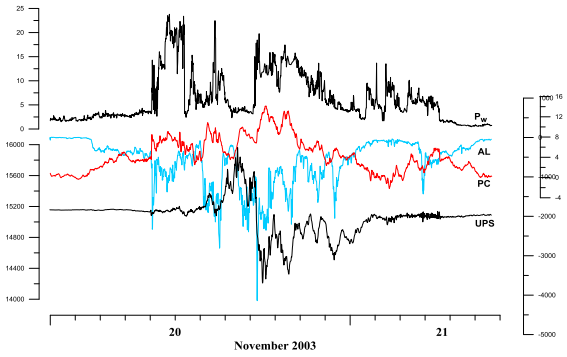

Fig. 4.6. Evolution of the solar wind dynamic pressure Pw, polar cap currents (PC index), auroral electrojet (AL index), and geomagnetic disturbance at a northern observatory (UPS), in case of the November 20-21, 2003 storm

Finally, as a next step in assessing the GIC hazard for the European territory, we calculated the maximum value of the electric field and its orientation at observatories of the network, for each storm considered in this study. Maps are presented in Fig. 4.7.

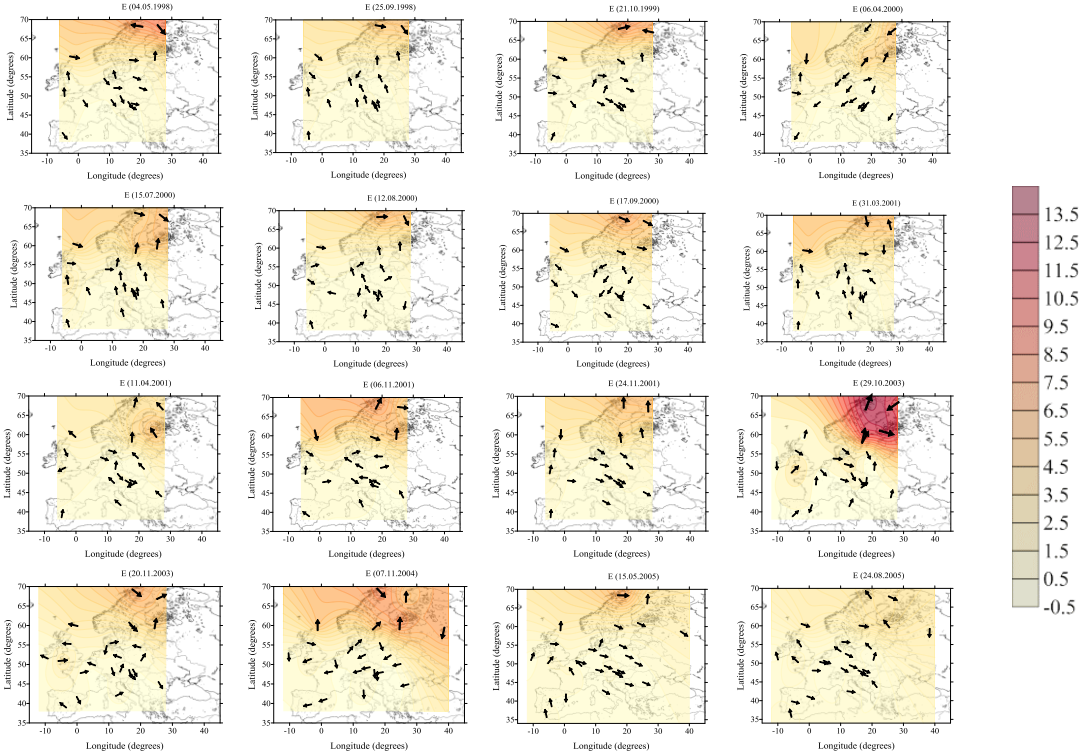

Fig. 4.7. Maps of the maximum geoelectric field induced at observatories of the European network, for each of the 16 geomagnetic storms of the present study

It is to be noted that the maximum E value is not reached at the same moment at all observatories and its orientation depends on that moment of the storm development.

4.3. Conclusions

Within the frame of the contract CNCSIS – UEFISCDI 93/2011, aspects of evaluating the geophysical effects of the major geomagnetic storms that occurred in the solar cycle 23 (1996-2008) have been tackled, as a first stage of solving the hazard induced by damaging electric currents in networks of electric energy and hydrocarbon transportation systems. Assessing induction currents in concrete technological networks is an engineering problem and needs inclusion of actual data regarding the network in the study.

References

Matandirotya, E., Cilliers, P. J., Van Zyl, R. R., 2015, Modelling geomagnetically induced currents in the South African power transmission network using the finite element method, Space Weather , doi: 10.1002/2014SW001135.

Viljanen, A. and Pirjola, R., 1989, Statistics on geomagnetically-induced currents in the Finnish 400 kV Power system based on recordings of geomagnetic variations, J. Geomag. Geoelectr., 41, 411-420.

Viljanen, A., Pirjola, R., Pracser, E., Katkalov, J., Wik, M., 2014, Geomagnetically induced currents in Europe, J. Space Weather Space Clim., 4, A09, doi: 10.1051/swsc/2014006.

Chapter V. Dissemination of results

In the report time-span the following papers have been submitted for publication:

- Besliu-Ionescu, D., Mierla, M., Maris Muntean, G., *Magnetic crochet associated to the seismically active flare of March 29, 2014*, Romanian Geophysical Journal, accepted, 2015.
- Besliu-Ionescu, D., Mierla, M., Maris Muntean, G., *The influence of April 10, 2001 CME on the Earth Magnetosphere*, Sun and Geosphere, submitted, 2015.
- Greculeasa, R., Dobrica, V., Isac, A., *The evolution of the geomagnetic field on the Romanian territory. Measurements in the secular variation national network between 2010 and 2014*, Romanian Geophysical Journal, accepted, 2015.
- Dobrica, V., Demetrescu, C., Stefan, C., Greculeasa, R., *Geophysically induced currents, a space weather hazard. Case study – Europe under intense geomagnetic storms of the solar cycle 23*, Sun and Geosphere, submitted, 2015.
- Stefan, C., Dobrica, V., Demetrescu, C., *Residual 11-year signal in coefficients of main field models*, Romanian Geophysical Journal, accepted, 2015.
- Dobrica, V., Demetrescu, C., Mandea, M., Geomagnetic field declination: from decadal to centennial scales, Journal of Geophysical Research B, 2015, submitted.

Also, during the year 2015 the contract members have participated to 5 international scientific meetings, with 17 papers:

- Besliu-Ionescu, D., Mierla, M., Dobrica, V., Maris Muntean, G., Magnetospheric Energy Input during Intense Geomagnetic Storms in SC23, *European Geosciences Union General Assembly, Vienna, Austria, 12 – 17 April 2015*
- Besliu-Ionescu, D., Mierla, M., Maris Muntean, G., The Influence of Apr 10, 2001 CME on the Magnetosphere, *The Seventh Workshop "Solar influences on the magnetosphere, ionosphere and atmosphere", Sunny Beach, Bulgaria, 1-5 June 2015*
- Besliu-Ionescu, D., Mierla, M., Maris Muntean, G., Energy coupling functions between the solar wind and the Earth magnetosphere, *Solar Variability and its Heliospheric Effects, Athens, Greece, 2-6 November 2015 (invited talk)*
- Besliu-Ionescu, D., Mierla, M., Study of energy input into the magnetosphere during SC23 intense geomagnetic storms, *12th European Space Weather Week, Ostend, Belgium, 23-27 November 2015*
- Demetrescu C., Dobrica V., Stefan C., Greculeasa, R., Surface electric field variations induced by intense geomagnetic storms of the solar cycle 23, a case study

for the European geomagnetic observatory network, *European Geosciences Union General Assembly, Vienna, Austria, 12 – 17 April 2015*

- Demetrescu C., Dobrica V., Stefan C., Greculeasa, R., Induced Currents, a space weather hazard. Case study – Europe under intense geomagnetic storms of the solar cycle 23, *The Seventh Workshop "Solar influences on the magnetosphere, ionosphere and atmosphere", Sunny Beach, Bulgaria, 1-5 June 2015*
- Demetrescu C., Dobrica V., The Quiet Sun of 1964-65 and the following solar cycle 20, an expression of long-term evolution of solar activity, *International Union of Geodesy and Geophysics General Assembly, Prague, the Czech Republic, 22 June – 02 July 2015*
- Demetrescu, C., Dobrica V., Stefan, C., Long-term evolution of the ring current as infered from geomagnetic data, *Asia Oceania Geosciences Society (AOGS) Assembly, Singapore, 02 – 07 August 2015*
- Demetrescu, C., Dobrica, V., Long- and short-term responses of the heliosphere-magnetosphere environment to solar activity variations, *Solar Variability and its Heliospheric Effects, Athens, Greece, 2-6 November 2015 (invited talk)*
- Dobrica, V., Pirloaga, R., Stefan, C., Demetrescu, C., On geoeffective solar variability signature in northern temperate climate zone at specific atmospheric levels, *European Geosciences Union General Assembly, Vienna, Austria, 12 – 17 April 2015*
- Dobrica, V., Demetrescu, C., Long-term evolution of geomagnetic activity. An analysis of its solar and magnetospheric sources, *International Union of Geodesy and Geophysics General Assembly, Prague, the Czech Republic, 22 June – 02 July 2015*
- Dobrica, V., Stefan, C., Demetrescu, C., On external signals in long time-span geomagnetic models, *MagNetE Workshop, Budapest, Hungary, 16-18 September 2015*
- Dobrica, V., Georgieva, K., Kirov, B., Demetrescu, C., Geomagnetic activity: long- and short-term variability, sources, *Solar Variability and its Heliospheric Effects, Athens, Greece, 2-6 November 2015 (invited talk)*
- Greculeasa R., Demetrescu, C., Dobrica, V., On the lateral distribution of electrical properties of crust and mantle in Europe, *European Geosciences Union General Assembly, Vienna, Austria, 12 – 17 April 2015*

- Greculeasa., R., Dobrica, V., Demetrescu, C., *Romanian secular variation network. Geomagnetic measurements 2013-2014, MagNetE Workshop, Budapest, Hungary, 16-18 September 2015*
- Stefan, C., Demetrescu, C., Dobrica, V., On the traveling speeds of the ~80-year variation field features at the top of the core, *International Union of Geodesy and Geophysics General Assembly, Prague, the Czech Republic, 22 June – 02 July 2015*
- Stefan, C., Dobrica, V., Demtrescu, C., Short-term variability of the magnetopause standoff distance, *International Union of Geodesy and Geophysics General Assembly, Prague, the Czech Republic, 22 June – 02 July 2015*

In the end, we mention that the project web page was updated accordingly. The address is http://www.geodin.ro/IDEI2011/engl/index.html.